20th AIAA Computational Fluid Dynamics Conference
27 - 30 June 2011, Honolulu, Hawaii

AIAA 2011-3217

Study of turbulence-chemistry interaction in hypersonic turbulent boundary layers

Lian Duan* and M. Pino Martín†

Department of Aerospace Engineering, University of Maryland, College Park, 20742

Studies of the turbulence-chemistry interaction (TCI) are performed in hypersonic turbulent boundary layers using direct numerical simulation (DNS) flow fields under typical hypersonic conditions representative of blunt-body and slender-body hypersonic vehicles, with supercatalytic and noncatalytic wall conditions in pure air. Nondimensional governing parameters, 'interaction' Damköhler number and relative heat release, are proposed to measure the influence of TCI on flow composition and temperature. Both *a priori* and *a posteriori* studies are performed to assess the effect of TCI on chemical production rates and mean and turbulence flow characteristics. In addition, an effective approach (called PDF-TS) to estimate the intensity of TCI based on 'laminar-chemistry' Reynolds averaged Navier-Stokes (RANS) mean flow solutions is presented, which combines an assumed probability density function (PDF) with a temperature fluctuation scaling (TS), and can be used to identify regions where TCI could be potentially important.

Nomenclature

w	chemical production rate, kg/m^{3}s, or wall-normal velocity, m/s
u	streamwise velocity, m/s
v	spanwise velocity, m/s
T	temperature, K
c	concentration, mol/m^3
Y	species mass fraction, dimensionless
W	molecular weight, kg/mol
ν	stoichiometric coefficient, dimensionless
k	reaction rate coefficient
K_{eq}	equilibrium constant
T_a	activation temperature
M	Mach number, dimensionless
ρ	density, kg/m^3
ns	total number of species, dimensionless
δ	boundary layer thickness, m
θ	momentum thickness, m
δ^*	displacement thickness, m
H	shape factor, $H = \delta^*/\theta$, dimensionless
q	heat flux, $q_j = -\kappa\frac{\partial T}{\partial x_j}$, J/(m^2·s), or turbulence kinetic energy, $q = \frac{u'^2+v'^2+w'^2}{2}$, m^2/s^2
C_p	heat capacity at constant pressure, J/(K·kg)
C_v	heat capacity at constant volume, J/(K·kg)
γ	specific heat ratio, $\gamma = C_p/C_v$, dimensionless
T_r	recovery temperature, $T_r = T_\delta(1 + 0.9 * \frac{\gamma-1}{2}M_\delta^2)$, K
u_τ	friction velocity, m/s
h	specific enthalpy, J/kg

*Current Address: Research Scientist, National Institute of Aerospace, Hampton, VA 23666
†Associate Professor, Department of Aerospace Engineering, Associate Fellow, AIAA

h° heat of formation, J/kg
p pressure, $p = \sum_s \rho_s \frac{\hat{R}}{M_s} T$, Pa
E total energy, J/m^3
μ mixture viscosity, kg/(m·s)
S_{ij} strain rate tensor, $S_{ij} = \frac{1}{2}(\partial u_i/\partial x_j + \partial u_j/\partial x_i)$, s^{-1}
σ_{ij} shear stress tensor, $\sigma_{ij} = 2\mu S_{ij} - \frac{2}{3}\mu\delta_{ij}S_{kk}$, Pa
κ mixture thermal conductivity, J/(K·m·s)
J diffusive mass flux, kg/m^2·s
Le Lewis number, dimensionless
Re_θ Reynolds number, $Re_\theta \equiv \frac{\rho_\delta u_\delta \theta}{\mu_\delta}$, dimensionless
$Re_{\delta 2}$ Reynolds number, $Re_{\delta_2} \equiv \frac{\rho_\delta u_\delta \theta}{\mu_w}$, dimensionless
Re_τ Reynolds number, $Re_\tau \equiv \frac{\rho_w u_\tau \delta}{\mu_w}$, dimensionless

Superscripts

$+$ inner wall units

Subscripts

∞ freestream
δ boundary layer edge
s chemical species
f forward reaction
b backward reaction
w wall variables
x streamwise spatial coordinates
y spanwise spatial coordinates
z wall-normal for spatial coordinates

I. Introduction

The boundary layers on hypersonic systems, including re-entry capsules and air-breathing vehicles, are turbulent and chemically reacting. Fluctuations in temperature and species composition cause fluctuations in species production rate $w_s(T, c)$. Because of the nonlinear dependence of w_s on its parameters, we have

$$\overline{w}_s(T, c) \neq w_s(\overline{T}, \overline{c})$$

and the difference is referred to as TCI, where overbar indicates a mean quantity.

It is well established today that in the field of combustion TCI significantly influences the turbulent mixing and the reaction of fuel and air at high speeds, and is important for predicting many flow quantities such as reaction rates and ignition delay.[1–7] The equivalent information is not yet known for hypersonic boundary layers. As a result, existing Reynolds-averaged-Navier-Stokes (RANS) calculations for hypersonic boundary layers have neglected the interrelationship between chemistry and turbulence, and the error introduced by such a simplification is largely uncertain.

Direct numerical simulations provide a vast amount of accurate data and have been used to analyze turbulent boundary layers at high Mach numbers. Most of the DNS studies have been carried out at low-enthalpy, non-reacting conditions. For example, DNS of nonreacting turbulent boundary layers have been performed by Guarini et al.[8] at Mach 2.5, Pirozzoli et al.[9] at Mach 2.25, Maeder et al.[10] at Mach 3, 4.5 and 6, Duan et al.[11] at Mach 5 with wall-to-freestream-temperature ratio varying from 1 to 5.4, Duan et al.[12] with freestream Mach number varying from 3 to 12, and Dong & Zhou[13] with Mach number varying from 2.5 to 6. An essential part of these DNS studies is to provide detailed turbulence statistics for checking the validity of empirical turbulence scalings as well as for developing turbulence models.

There are only limited DNS studies of turbulent boundary layers at high enthalpy conditions including with chemical reactions. Almost all previous DNS studies of chemically reacting turbulent boundary layers focused on the difference between reacting and non-reacting boundary layers, and have shown that chemical reactions significantly influence flow quantities such as mean and RMS velocity and temperature, skin friction and surface heat flux.[14–17] However, the direct effects due to the differences between $\overline{w}_s(T, c)$ and $w_s(\overline{T}, \overline{c})$ have not been fully explored.

In the current study, we assess the significance of TCI in turbulent boundary layers under typical hypersonic conditions by *a priori* and *a posteriori* studies using DNS data. Both the influence of turbulent fluctuations on the chemical production rates, and the influence of the modified chemical production rates on the mean and turbulent quantities will be investigated. In addition, an effective approach (called PDF-TS) to estimate the intensity of TCI based on 'laminar-chemistry' Reynolds averaged Navier-Stokes (RANS) mean flow solutions is presented, which combines an assumed probability density function (PDF) with a temperature fluctuation scaling (TS), and can be used to identify regions where TCI could be potentially important.

The paper is structured as follows. Flow conditions and simulation details appear in Sections II and III, respectively. The production rate calculation for finite-rate chemistry in chemically reacting flow is given in Section IV. Non-dimensional governing parameters for TCI are proposed in Section V. *A priori* and *a posteriori* studies of TCI using DNS data are given in Section VI. The PDF-TS method is introduced in Section VII. Finally, conclusions are drawn in Section VIII.

II. Flow condition

We consider the boundary layer on a lifting-body consisting of a flat plate at an angle of attack, which flies at an altitude of 30km with a Mach number 21. Two different inclined angles, 35° and 8°, are considered, denoted as Wedge35 and Wedge8, respectively. For the case Wedge35, the angle of attack is sufficiently large that the flow behind the shock attains a temperature high enough to produce chemical reactions, and the boundary layer is representative of those on a blunt-body hypersonic vehicle. For the case Wedge8, the angle of attach is small so that the flow at the edge of the boundary layer is cold and non-reacting. Within the boundary layer the temperature rises due to the recovery effects and the flow is partially dissociated. The boundary layer in this case is typical of those on a slender-body hypersonic vehicle. For both cases, the boundary layer conditions for the DNS domain are established by extracting them from a larger domain finite-volume RANS calculation using DPLR,[18] which is obtained using five-species-air-reaction mechanism, Equation 5 below, and considers chemical processes of 5 species: N_2, O_2, NO, N, O. The flow conditions for RANS are given in Table 1. Figure 1 shows the entire computational domain for RANS calculation and the DNS subdomain identified to explore turbulence-chemistry interaction for both conditions. In order to investigate the influence of species boundary conditions on TCI, we consider both 'supercatalytic' and 'noncatalytic' surface-catalytic models for each flow conditions. The supercatalytic and noncatalytic surface-catalytic models used in the current analysis are representative of the extreme conditions that might happen at the surface of a re-entry flight. The details of surface-catalytic model and species boundary conditions are discussed in Section III.B. For simplicity, we refer to Wedge35 with supercatalytic wall as Wedge35supercata, Wedge35 with noncatalytic wall as Wedge35noncata. Similar definitions are used for case Wedge8. Table 2 lists the boundary layer edge conditions and wall parameters for all DNS cases.

M_∞	ρ_∞(kg/m^3)	T_∞(K)	T_w(K)
21	0.0184	226.5	2400.0

Table 1. Freestream and wall parameters for the larger domain finite-volume RANS calculation

Cases	M_δ	ρ_δ(kg/m^3)	T_δ(K)	T_w(K)	T_w/T_r	Re_θ	Re_τ	$Re_{\delta 2}$	θ(mm)	H	δ(mm)
Wedge35supercata	3.44	0.175	4456.5	2400.0	0.20	966.2	906.4	1544.5	0.154	1.79	1.397
Wedge35noncata	3.43	0.175	4464.9	2400.0	0.20	1001.1	978.5	1661.7	0.173	2.17	1.746
Wedge8supercata	10.3	0.0834	948.1	2400.0	0.15	3195.1	859.7	2069.2	0.389	15.4	10.3
Wedge8noncata	10.3	0.0834	948.1	2400.0	0.15	3058.1	741.0	1941.0	0.360	14.9	8.87

Table 2. Dimensional bounday layer edge and wall parameters for direct numerical simulations

III. Simulation details for DNS

III.A. Governing equations, constitutive relations and numerical methods

The governing equations, constitutive relations and numerical method for DNS of chemically reacting flow are described in detail in our previous paper.[19] Therefore, only a cursory description is given here.

The equations describing the unsteady motion of a reacting fluid are given by the species mass, mass-averaged momentum, and total energy conservation equations, which, neglecting thermal non-equilibrium, are

$$\begin{aligned}
\frac{\partial \rho_s}{\partial t} + \frac{\partial}{\partial x_j}\Big(\rho_s u_j + J_{sj}\Big) &= w_s \\
\frac{\partial \rho u_i}{\partial t} + \frac{\partial}{\partial x_j}\Big(\rho u_i u_j + p\delta_{ij} - \sigma_{ij}\Big) &= 0 \\
\frac{\partial E}{\partial t} + \frac{\partial}{\partial x_j}\Big((E+p)u_j - u_i\sigma_{ij} + q_j + \sum_s J_{sj}h_s\Big) &= 0
\end{aligned} \tag{1}$$

The thermodynamic properties of high-temperature air species for evaluating total energy E and species enthalpy h_s are computed by NASA Lewis curve fits.[20] Mixture transport properties μ and κ for evaluating stress tensor σ_{ij} and heat flux q_j are calculated using the Gupta[21]-Yos[22] mixing rule. Fick's diffusion model with unity Lewis number is used for calculating species diffusion flux J_{sj}. The gas-phase reaction mechanism and the formula for evaluating species production rate w_s are introduced in detail in Section IV.

For numerical discretization, we use a linearly and non-linearly optimized, 4th-order-accurate weighted essentially-non-oscillatory (WENO) method[23,24] for convective terms, which is a high-order shock-capturing scheme with optimal bandwidth efficiency and minimum numerical dissipation. We use 4th-order-accurate central difference scheme for viscous term and 3rd-order-accurate low-storage Runge-Kutta method[25] for time integration, as in Martín[26] and Duan & Martín.[19]

III.B. Initial and boundary conditions

The initial DNS flow field is obtained by first exacting the mean profiles from the RANS calculation at the location indicated in Figure 1, and then superimposing the fluctuating field. The fluctuating field is obtained by transforming that of an incompressible turbulent boundary layer DNS using well-established scaling laws. The details of this initialization technique are introduced by Martín.[26]

On the wall boundary, non-slip conditions are used for the three velocity components. The wall temperature is prescribed and kept isothermal. The flow condition on the top boundary are fixed edge conditions which are extracted from the RANS calculation. Periodic boundary conditions have been used in the streamwise and spanwise directions.

We consider two extreme cases for species boundary conditions. The first case is so-called 'noncatalytic' wall, which assumes no atom recombination and minimal enthalpy recovery at the surface. The species boundary condition for noncatalytic wall is

$$\left(\frac{\partial Y}{\partial n}\right)_{s,w} = 0 \tag{2}$$

with n the unit vector in the wall normal direction.

The other extreme case is the so-called 'supercatalytic' wall, which assumes infinitely fast atom recombination and maximum enthalpy recovery at the surface. In this case, the chemical composition at the wall recovers to that in the freestream and the species boundary condition is simply

$$Y_{s,w} = Y_{s,\infty} \tag{3}$$

Note, $Y_{s,\infty}$ is the flow composition for the cold air upstream of the leading-edge shock and may be different from the post-shock boundary layer edge composition $Y_{s,\delta}$.

III.C. Numerical simulation parameters

The computational domain size and grid resolution are determined based on the characteristic large length scale, δ, and the characteristic small, near-wall length scale, z_τ, respectively. The computational domain is chosen to be large enough to contain a good sample of the large scales, while the grid resolution is fine enough to resolve the near wall structures.[26] The domain size ($L_x \times L_y \times L_z$), the grid size ($\Delta x \times \Delta y \times \Delta z$) and the number of grid points ($N_x \times N_y \times N_z$) are given in Table 3. We use uniform grids in the streamwise and spanwise directions as Δx^+ and Δy^+, and geometrically stretched grids in the wall-normal direction, with $z_k = z_2(\alpha^{k-1} - 1)/(\alpha - 1)$.

Cases	L_x/δ	L_y/δ	L_z/δ	Δx^+	Δy^+	z_2^+	α	N_x	N_y	N_z
Wedge35supercata	17.2	1.7	4.3	26.6	4.0	0.19	1.068	576	384	110
Wedge35noncata	13.5	1.4	3.4	23.0	3.5	0.17	1.068	576	384	110
Wedge8supercata	17.7	2.5	5.1	26.5	5.7	0.26	1.067	576	384	110
Wedge8noncata	20.0	2.9	5.7	25.7	5.5	0.25	1.067	576	384	110

Table 3. Grid resolution and domain size for the direct numerical simulation.

To assess the adequacy of the domain size, streamwise and spanwise two-point correlation for the streamwise, spanwise and wall-normal velocity components are plotted. Figure 2 plots the streamwise and spanwise two-point correlations at $z^+ = 15$ and $z/\delta = 0.1$ for case Wedge35supercata. The two-point correlations drop to zero for large separations, indicating the computational domain is large enough to contain a good sample of the large scales. Similar results can be shown for other cases. Notice that cases with lower T_w/T_r require larger flow domains as a result of heat transfer effects, as described in.[11]

The grid resolution can be assessed by grid-convergence study. Figure 3(a-d) plot the mean temperature, mean species mass fraction, r.m.s temperature and r.m.s species mass fraction with different number of grid points for case Wedge35supercata. All the corresponding curves collapse to within 1%, indicating the grid is fine enough to converge the results. Grid convergence has been checked for all the other cases.

The averages of all the turbulence statistics are computed over streamwise and spanwise directions of each field; then an ensemble average is calculated over fields spanning around one non-dimensional time unit. The time is non-dimensionalized by δ/u_τ, which corresponds to around 20 large-eddy turnover time. Both Reynolds and Favre averaging are used. The Reynolds average f over the $x-$ and $y-$directions will be denoted by $\bar{f}$, or $< f >$, and fluctuations about this mean will be denoted by f'. The Favre average over the $x-$ and $y-$directions,$\tilde{f}$, is a density-weighted average:

$$\tilde{f} = \frac{\overline{\rho f}}{\overline{\rho}} \tag{4}$$

Fluctuations about the Favre average will be denoted by f''.

At the selected flow conditions, the temperature is high enough to partially dissociate the flow, as shown in Figures 4(a,b) where the mean temperature and the mass fractions of atomic oxygen are plotted. In addition, Figures 5(a,b) show that the levels of fluctuation magnitude in both temperature and species compositions for all cases.

IV. Chemical production term

IV.A. Gas-phase reactions for Earth atmosphere

For gas-phase reactions, The gas-phase reactions in DNS are modeled using air-five-species mechanism: N_2, O_2, NO, N, and O with Arrhenius parameters,[27] shown as follows:

$$\begin{aligned} N_2 + M &\rightleftharpoons 2N + M \\ O_2 + M &\rightleftharpoons 2O + M \\ NO + M &\rightleftharpoons N + O + M \\ N_2 + O &\rightleftharpoons NO + N \end{aligned}$$

$$\mathrm{NO} + \mathrm{O} \quad \rightleftharpoons \quad \mathrm{O_2} + \mathrm{N} \tag{5}$$

The reacting mechanism represents the realistic reactions of air before ionization happens, which is a good approximation at temperatures less than about $10,000$K. The corresponding equilibrium constants are computed from the Gibbs free energy as functions of temperature and then fitted to Park (1990) expressions.[27]

IV.B. General formulation for w_s

For a reaction

$$\sum_{i=1}^{ns} \nu_i' M_i \rightleftharpoons \sum_{i=1}^{ns} \nu_i'' M_i \tag{6}$$

The chemical production rate w_s can be defined by the law of mass action to be

$$w_s = W_s(\nu_s'' - \nu_s')(\omega_f - \omega_b) = W_s(\nu_s'' - \nu_s') \left(k_f \prod_{i=1}^{ns} c_i^{\nu_i'} - k_b \prod_{i=1}^{ns} c_i^{\nu_i''} \right) \tag{7}$$

where ν_i' and ν_i'' are the stoichiometric coefficients of the reactants and products, respectively. ω_f and ω_b are independent of particular species and can be taken as the reaction rates of the forward and backward reactions, respectively. The forward reaction rate coefficient k_f can be determined from the Arrhenius expression

$$k_f = AT^b exp\left(-\frac{T_a}{T}\right) \tag{8}$$

where A and b are constants. The backward reaction rate coefficient is given by

$$k_b = \frac{k_f}{K_{eq}} \tag{9}$$

where the equilibrium constant K_{eq} is a function of T and can be determined using curve fits.[27]

Equations 7,8,9 show that $w_s(T, c)$ depends nonlinearly on its parameters (primarily temperature). As a result, $\overline{w_s(T,c)}$ is usually different from $w_s(\overline{T}, \overline{c})$. The former can be referred as the 'turbulent' reaction rate, in which turbulence fluctuations, including both temperature and species fluctuations, have been taken into account, and the latter can be referred as 'laminar' reaction rate (although $\overline{T}$ and $\overline{c_i}$ are mean turbulent profiles), which we would obtain if there were no turbulent fluctuations. The greater the difference between the two, the more significant TCI is.

V. Governing parameters for TCI

The difference between $\overline{w_s(T,c)}$ and $w_s(\overline{T}, \overline{c})$ is a measure of TCI intensity and indicate how chemical production rates get augmented due to turbulent fluctuation. In order to further predict how such augmentation effects influence the overall turbulent flow field, we propose the nondimensional parameters based on the flow governing equations.

Finite-rate chemical reactions act as sources for the production of species in species continuity equations as well as heat production in the energy equation. To estimate the species and heat production effects by TCI, we introduce species 'interaction' Damköhler number Da_s^I and 'interaction' relative heat release $\overline{\Delta h}^I$, which is defined as

$$Da_s^I \equiv \left| \frac{\left(\overline{w_s(T,c)} - w_s(\overline{T}, \overline{c}) \right) \tau_t}{\overline{\rho}_s} \right|, \quad \overline{\Delta h}^I \equiv \frac{\sum_{i=1}^{ns} \left(\overline{w_i(T,c)} - w_i(\overline{T}, \overline{c}) \right) h_i^\circ \tau_t}{\sum_{i=1}^{ns} \overline{\rho}_i \left(h_i(\overline{T}) + \frac{1}{2} \overline{u}_k \overline{u}_k \right)} \tag{10}$$

In both definitions, τ_t is some turbulence time scale, the choice of which may be large-eddy turnover time $\frac{\delta}{U_\delta}$, or $\frac{q}{\epsilon}$, which is the time scale for energy-containing eddies, and $\left| \overline{w_s(T,c)} - w_s(\overline{T}, \overline{c}) \right|$ is included to measure the intensity of TCI. Positive values of relative heat release indicate endothermicity, whereas positive indicate exothermicity of the chemistry mechanism due to TCI.

The species 'interaction' Damköhler number is the ratio of TCI species mass production during the characteristic flow time to species total mass, and provides a measure of mass production effects by TCI. The 'interaction' relative heat release is the ratio of TCI chemical heat release during the characteristic flow time to the total flow enthalpy, and provides a measure of heat production effects by TCI. If the magnitude of Da_s^I is close to or larger than unity, a significant change in flow composition by TCI is expected. When $\overline{\Delta h}^I$ is large, a large influence of TCI on the thermal field is expected.

The definitions of the species 'interaction' Damköhler number and 'interaction' relative heat release bear an analogy with the definitions of the Damköhler number and relative heat release by Martin & Candler,[28,29] which have been found to be important parameters that govern the influence of chemistry on the turbulent flow field.

In order to investigate the relative importance of temperature TCI alone, on chemical mass and heat production, Da_s^I and $\overline{\Delta h}^I$ are defined as

$$Da_s^I \equiv \left| \frac{\left(\overline{w_s(T,\overline{c})} - w_s(\overline{T},\overline{c}) \right) \tau_t}{\overline{\rho}_s} \right|, \quad \overline{\Delta h}^I \equiv \frac{\sum_{i=1}^{ns} \left(\overline{w_i(T,\overline{c})} - w_i(\overline{T},\overline{c}) \right) h_i^\circ \tau_t}{\sum_{i=1}^{ns} \overline{\rho}_i \left(h_i(\overline{T}) + \frac{1}{2}\overline{u}_k\overline{u}_k \right)} \tag{11}$$

where $\overline{w_s(T,c)}$ in Equation 10 has been substituted by $\overline{w_s(T,\overline{c})}$.

VI. Assessment of TCI in hypersonic turbulent boundary layers

VI.A. *a priori* study

In the *a priori* study, the 'turbulent' reaction rate $\overline{w(T,c)}$ and 'laminar' reaction rate $w(\overline{T},\overline{c})$ are calculated and compared using the DNS data.

Figure 6 plots the 'turbulent' and 'laminar' production rates of each species for the case Wedge35 with supercatalytic and noncatalytic species boundary conditions. There are distinguishable differences between the mean 'turbulent' and 'laminar' production rates for both supercatalytic and noncatalytic walls. For species N_2, O_2, N and O, the maximum relative difference is larger than 30%. Similar differences also exist for the case Wedge8, as shown in Figure 7.

The high sensitivity of chemical production rates to turbulence fluctuations can be understood by the fact that $w_s(T,c)$ depends nonlinearly on its parameters (primarily temperature), as indicated in Equation 8, and for air reactions T_a is typically an order of magnitude larger than the flow temperature.

To predict the effect of TCI on the turbulence flow field, Figure 8 plots the 'interaction' Damköhler number and 'interaction' relative heat release. It is shown that Da_s^I for all species except N and $\overline{\Delta h}^I$ are at least one order smaller than unity, indicating that TCI has little influence on the overall flow composition as well as temperature and velocity field. The fact that Da_N^I is $o(1)$ might suggest that TCI will have a significant influence on Y_N. However, given that Y_N is very small across the boundary layer, the variation in Y_N is expected to have little influence on the overall flow composition.

VI.B. *a posteriori study*

TCI is further assessed by performing *a posteriori* study. In *a posteriori* study, the effect of TCI is investigated by comparing results of the original DNS with an 'artificial' DNS, in which the effect of TCI has been neglected. The 'artificial' DNS is performed with chemical source term $w(T,c)$ evaluated as $w(\overline{T},\overline{c})$ while keeping all the other conditions the same.

Figure 9 and Figure 10 plot the mean mass fraction and RMS of mass fraction for all cases. It is shown that significant differences in $\overline{Y}_N$ for cases Wedge8supercata and Wedge8noncata with and without TCI, consistent with the fact that Da_N^I for these cases are close to unity for most of the boundary layer, as seen in Figure 8. Slight decreases in $\overline{Y}_{NO}$ and $\overline{Y}_O$ are also observed for the case Wedge8supercata, which is consistent with the fact that Da_{NO}^I and Da_O^I has relatively larger values for Wedge8supercata than other cases. For the RMS of species mass fraction, significant differences can be observed for nearly all the species. Figure 9 and Figure 10 indicate that TCI may influence the detailed chemical compositions of the turbulent flow field. However, Figure 11 shows that TCI has subtle difference in both mean flow density and RMS of flow density.

To further investigate the influence of TCI on flow dynamics, Figure 12 plots the mean velocity profile and the turbulent kinetic energy (TKE). It is shown that both the mean velocity and TKE are nearly the same with and without TCI for all cases, indicating negligible influence of TCI on the velocity field.

In terms of the temperature field, Figure 13 and Figure 14 plot the mean temperature and the RMS of temperature fluctuation for the cases Wedge35 and Wedge8, respectively. It is shown that there is nearly no difference in mean temperature with and without TCI for all cases, consistent with the small values of $\overline{\Delta h^I}$, as shown in Figure 8. For the temperature fluctuation, a reduction as large as 10% is observed when TCI is included. The slightly larger decrease in $T'_{rms}/\bar{T}$ for the case Wedge35 than Wedge8 is consistent with the relatively larger value of $\overline{\Delta h^I}$ for Wedge35.

To demonstrate the influence of TCI on turbulent transport of momentum and heat, Figure 15 plots normalized Reynolds shear stress and turbulent heat flux with and without TCI for all cases. It is shown that TCI has subtle influence on Reynolds shear stress and turbulent heat flux. In terms of Reynolds mass flux, Figure 16 shows that for Wedge8supercata and Wedge8noncata the maximum varation in Reynolds mass flux due to TCI is as large as 40%, indicating that TCI influences the turbulent transport of species mass fraction and is consistent with the change in flow composition for these cases.

To demonstrate the influence of TCI on surface skin friction, heat flux and pressure loading, Table 4 provides C_f, $\overline{q}_w$, $q'_{w,rms}/\overline{q}_w$, $\overline{p}_w$ and $p'_{w,rms}/\overline{p}_w$ with and without TCI for all cases. It is shown that TCI has negligible influence on all of these quantities.

Case	C_f	$\overline{q}_w$	$q'_{w,rms}/\overline{q}_w$	$\overline{p}_w$	$p'_{w,rms}/\overline{p}_w$
Wedge35supercata, with TCI	3.82×10^{-3}	2.99×10^{7}	0.45	2.61×10^{5}	0.10
Wedge35supercata, without TCI	3.81×10^{-3}	2.98×10^{7}	0.44	2.61×10^{5}	0.10
Wedge35noncata, with TCI	3.62×10^{-3}	2.32×10^{7}	0.52	2.62×10^{5}	0.08
Wedge35noncata, without TCI	3.63×10^{-3}	2.33×10^{7}	0.52	2.62×10^{5}	0.08
Wedge8supercata, with TCI	1.06×10^{-3}	0.43×10^{7}	0.64	0.24×10^{5}	0.29
Wedge8supercata, without TCI	1.07×10^{-3}	0.43×10^{7}	0.65	0.24×10^{5}	0.29
Wedge8noncata, with TCI	1.04×10^{-3}	0.41×10^{7}	0.68	0.24×10^{5}	0.29
Wedge8noncata, without TCI	1.04×10^{-3}	0.42×10^{7}	0.68	0.24×10^{5}	0.30

Table 4. Skin friction, mean and RMS of heat flux and pressure loading. The units of $\overline{q}_w$ and $\overline{p}_w$ are W/m^2 and Pa, respectively.

VII. PDF-TS method

The evaluation of the governing parameters (Equations 10) depends on the knowledge of $\overline{w(T,c)}$, which is not readily available from a typical RANS simulation. In addition, due to the large extent of the parameter space, including permutations of flow conditions, atmospheric and added- or wall-catalytic chemical mechanisms, and the small subset of those that have been explored so far, it would be useful to have a method to predict the intensity of TCI in the context of RANS, before actually doing more expensive simulations such as DNS, or taking extra efforts to include TCI models, since high-order modeling approaches like DNS and LES are computationally intensive, and the use of steady-state RANS models is the tool of choice for routine design purposes.[30]

Martin & Candler[28,29] noticed that for external hypersonic air flows, the chemical source term has a strong temperature dependence. This can be seen by representing the variables as the mean and fluctuating quantities: $T = \overline{T} + T'$ and $c_s = \overline{c}_s + c'_s$. Taking one of the predominant air reactions, binary dissociation of nitrogen $N_2 + M \rightarrow 2N + M$, the source term to a first order approximation in fluctuating quantities is

$$w_{\mathrm{N}_2} = \overline{w}_{\mathrm{N}_2} + \overline{w}_{\mathrm{N}_2} \left(\left(\frac{T_a}{\overline{T}} + b \right) \frac{T'}{\overline{T}} + \frac{c'_{\mathrm{N}_2}}{c_{\mathrm{N}_2}} + \frac{c'_{\mathrm{M}}}{\overline{c}_{\mathrm{M}}} \right) + \ldots \tag{12}$$

where b is the constant in Equation 8 and $\overline{w} = w(\overline{T}, \overline{c})$. The variations of w_{N_2} caused by temperature fluctuations may be especially large because T_a is an order of magnitude larger than typical flow temperatures.

In this section, we introduce the PDF-TS method for estimating the effects of temperature fluctuations on chemical production rates, or temperature TCI, in the context of RANS. The method combines an assumed PDF[2,6,31,32] with a temperature fluctuation scaling. The assumed PDFs are Gaussian or Beta distributions, which require values for the first and second moments. The first moment is available from solving the RANS equations, and a temperature scaling (TS) is derived to relate the second moment to the first. In the rest of the paper, we name this approach as PDF-TS, i.e. PDF with temperature scaling, for simplicity.

VII.A. Assumed PDF forms and parameters

The influence of temperature fluctuation on $\overline{w_s(T,c)}$ manifests itself in $\overline{k(T)}$, where k can be either k_f or k_b, and $\overline{k(T)} \neq k(\overline{T})$. The reaction rate coefficients $\overline{k(T)}$ can be evaluated by the assumed PDF approach, i.e.

$$\overline{k(T)} = \int_0^\infty k(T)P(T)dT \tag{13}$$

where $P(T)$ is the PDF of T. Several forms of $P(T)$ have been proposed by multiple researchers,[2,6,31,32] including the Gaussian PDF and the β PDF. The Gaussian PDF is given by

$$P(T) = \frac{1}{\sqrt{2\pi T''^2_{rms}}} exp\left[-\frac{(T-\overline{T})^2}{2T''^2_{rms}}\right] \tag{14}$$

Thus, the Gaussian PDF is completely determined by $\overline{T}$ and T''^2_{rms}, or $\overline{T}$ and temperature intensity $\frac{T'_{rms}}{\overline{T}}$.

The β PDF is given by

$$P(r) = \frac{r^{\beta_1-1}(1-r)^{\beta_2-1}}{\Gamma(\beta_1)\Gamma(\beta_2)}\Gamma(\beta_1+\beta_2) \tag{15}$$

where Γ is the gamma function and

$$\beta_1 = \overline{r}\left[\frac{\overline{r}(1-\overline{r})}{\overline{r'r'}} - 1\right]$$

$$\beta_2 = (1-\overline{r})\left[\frac{\overline{r}(1-\overline{r})}{\overline{r'r'}} - 1\right]$$

with $0 < r < 1$. The r in the Equation 15 is related to temperature by the following transformation

$$r = \frac{T - T_{min}}{T_{max} - T_{min}} \tag{16}$$

The transformation gives

$$\overline{r} = \frac{\overline{T} - T_{min}}{T_{max} - T_{min}} \tag{17}$$

and

$$\overline{r'r'} = \frac{T''^2_{rms}}{(T_{max} - T_{min})^2} \tag{18}$$

Thus, the β PDF is completely determined from $\overline{T}$, T''^2_{rms}, T_{min} and T_{max}.

The Gaussian pdf and β pdf are completely specified by the mean temperature and temperature fluctuation variance.

VII.B. Temperature fluctuation scaling in hypersonic boundary layers

Both the mean temperature and temperature fluctuation variance are needed to specify the assumed Gaussian or Beta PDFs, as shown in Subsection VII.A. The mean temperature is readily available from the solutions of RANS equations. An additional temperature fluctuation scaling is introduced to connect temperature fluctuation intensity with the flow quantities that can be evaluated using RANS solutions.

Here, we use a generalized version of Huang's strong Reynolds analogy[33] (HSRA) to relate the temperature fluctuation intensity to the streamwise velocity fluctuation intensity. HSRA has been validated and widely used for non-reacting hypersonic boundary layers with adiabatic and non-adiabatic walls,[8,10–12] By removing calorically perfect gas assumption used in the derivation, HSRA can be generalized for flows with

variable heat capacities and chemical reactions.[34] A cursory description of the derivation of the generalized HSRA is given below.

First, the temperature fluctuations and velocity fluctuations are related using the 'mixing length' relation:[33,35]

$$l_u \propto u'_{rms}/\left|\partial\overline{u}/\partial z\right|, \quad l_T \propto T'_{rms}/\left|\partial\overline{T}/\partial z\right| \tag{19}$$

where l_u and l_T are turbulent mixing length for velocity and temperature, respectively. With $l_u/l_T = Pr_t$,[33] we have

$$T'_{rms} = f(u'_{rms}) = \left|\frac{1}{Pr_t}\frac{\partial\overline{T}}{\partial\overline{u}}\right| u'_{rms} \tag{20}$$

Since for most cases it is the turbulent kinetic energy q rather than the streamwise turbulence intensity u'_{rms} that is readily available in the context of RANS calculations,[36] we further relate the streamwise turbulence intensity u'_{rms} in Equation 20 to the turbulent kinetic energy q by

$$u'_{rms} = C_M\sqrt{q} \tag{21}$$

with C_M is the proportionality factor. The value of C_M is related to the anisotropy ratios v'_{rms}/u'_{rms} and w'_{rms}/u'_{rms}, which have been found to be insensitive to freestream Mach number, wall temperature and enthalpy conditions.[11,12,34]

After combining Equations 20 and 21, we get a scaling for the temperature fluctuation intensity as

$$T'_{rms} = C_M\left|\frac{1}{Pr_t}\frac{\partial\overline{T}}{\partial\overline{u}}\right|\sqrt{q} \tag{22}$$

Equation 22 can be used to evaluate T'_{rms} in the context of typical RANS solutions. The right-hand-side of Equation 22 includes mean quantities as well as the turbulent kinetic energy q and turbulent Prandtl number Pr_t, all of which are available in the context of typical RANS calculations, such as standard $k-\varepsilon$ model with the gradient transport model.[30,36]

VII.C. Combining PDF with TS

The steps for using PDF-TS are summarized as follows:

1. Evaluate T'_{rms} using the temperature scaling (Equation 22)
2. Calculate reaction rate coefficients $\overline{k(T)}$ for each reactions using formula 13 with $P(T)$ being Gaussian or Beta distribution function.
3. Estimate 'turbulent' species production rates $\overline{w_s(T,\overline{c})}$ using the formula

$$\overline{w_s(T,\overline{c})} = W_s(\nu''_s - \nu'_s)\left(\overline{k_f(T)}\prod_{i=1}^{ns}\overline{c}_i^{\nu'_i} - \overline{k_b(T)}\prod_{i=1}^{ns}\overline{c}_i^{\nu''_i}\right) \tag{23}$$

4. Compute temperature TCI intensity $\overline{w(T,\overline{c})} - w(\overline{T},\overline{c})$ as well as the governing parameters Da_s^I and $\overline{\Delta h^I}$ using Equation 11

VII.D. PDF-TS evaluation and comparison with DNS data

To demonstrate the performance of various assumed forms of temperature PDFs, Figure 17 plots $\overline{k(T)}$ calculated by averaging DNS flow fields or following Equation 13 using Gaussian or Beta PDF for reactions $R1$ to $R5$. The integrations in Equation 13 for both forms of pdf are numerically performed between $T_{min} = \overline{T} - 3T'_{rms}$ and $T_{max} = \overline{T} + 3T'_{rms}$.[32] The results are insensitive to the shape of the PDF for all the cases, similar to the observations by Baurle[37] and Bray & Moss[38] for combustion flows. The match between PDF and DNS results is excellent throughout the boundary layer for Wedge35 cases. For Cases Wedge8, good agreement is achieved for $\frac{z}{\delta} \leq 0.6$. At $\frac{z}{\delta} > 0.6$, where $\overline{T}$ is relatively small and there is nearly no chemical reactions, the PDF results underpredict the correct results.

In terms of the performance of the temperature scaling, Figure 18 plots $\frac{T'_{rms}}{\overline{T}}$ calculated by averaging DNS flow fields or following Equation 20 for all DNS cases. It is shown that reasonable match between

the two is achieved through most of the boundary layer. In particular, the temperature fluctuation scaling correctly predicts the peak location and the general shape of temperature fluctuation intensity. The poor performance of Equation 20 near the peak location of $\overline{T}$, or the crossover location, where $\frac{\partial \overline{T}}{\partial z} = 0$ can be understood by the fact that the 'mixing length' assumption, where $l_T = T'_{rms}/(\partial \overline{T}/\partial z)$, no longer holds at $\frac{\partial \overline{T}}{\partial z} \approx 0$.

The insensitivity of the proportionality factor C_M with flow conditions can be demonstrated by DNS results across a wide range of freestream Mach number, wall temperature and enthalpy conditions, as it is shown in Figure 19. Through most of the boundary layer, C_M can be well approximately as

$$C_M = \frac{\sqrt{2}}{\sqrt{1 + C(1 - e^{-D(z/\delta)})^2}} \tag{24}$$

with $C = 1.06$, $D = 15$.

To demonstrate the overall performance of PDF-TS, Figure 20 and Figure 21 plot 'interaction' Damköhler number Da_s^I and relative heat release $\overline{\Delta h}^I$, respectively, computed by averaging DNS flow fields and PDF-TS method for various DNS cases. The PDF-TS method combines the Gaussian PDF given by Equation 14 and the temperature scaling given by Equation 22 with $Pr_t = 1.0$ and the value C_M given by Equation 24. It is shown that overall PDF-TS method predicts the governing parameters to the right order through most of the boundary layer. In particular, it correctly captures the peak locations as well as the peak values for various DNS cases. In addition, the relatively poor performance of PDF-TS is observed near $\frac{\partial \overline{T}}{\partial z} \approx 0$ due to the failure of the temperature scaling (Equation 22).

The validation of the assumed PDFs, the temperature scaling and PDF-TS has been performed against DNS data in different downstream locations along the wedge, and similar performances has been observed.

VII.E. Summaries and Comments

PDF-TS is a predictive method to estimate the intensity of TCI in hypersonic boundary layers based on 'laminar-chemistry' RANS calculations. It gives the sensitivity of chemical production rates to temperature fluctuations, as well as an order-of-magnitude estimate of the relative importance of temperature TCI after combined with the definitions of the governing parameters Da_s^I and $\overline{\Delta h^I}$, thus can provide guidance on whether or not to undertake further efforts to model TCI under selected flow conditions.

It should be noted that so far only the temperature fluctuation effects of TCI has been considered in PDF-TS, based on the general consideration that the chemical reactions for hypersonic external flows are overall endothermic and dominated by the dissociation of nitrogen and oxygen molecules. These reactions are characterized by very large activation energy with T_a typically an order of magnitude larger than the maximum flow temperature. As a result, the reaction rate is extremely sensitive to temperature variations, as indicated by the exponential relation in Equation 8. For situations when the species composition fluctuations are equally or more important, the current method provides only a subset of total regions with significant TCI, and the inclusion of species composition fluctuations may be necessary in order to give a more comprehensive evaluation of TCI.

VIII. Conclusions

We conduct direct numerical simulations to assess the effects of turbulence-chemistry interaction in hypersonic turbulent boundary layers, under typical hypersonic conditions representative of blunt-body and slender-body vehicles for Earth re-entry. Both 'supercatalytic' and 'noncatalytic' species boundary conditions are considered for each of flow conditions. *A priori* and *a posteriori* studies using DNS database show that the chemical production rate of individual species are significantly augmented by turbulent fluctuations, and TCI influences the turbulent transport of species mass fraction and the detailed chemical composition of the flow. However, in pure air, TCI has no sizable influence on most of the flow quantities, including the mean velocity and turbulent kinetic energy, Reynolds shear stress and turbulent mass flux, mean and RMS of density and temperature as well as surface skin friction, heat transfer and pressure loading. Similar studies at various Mach numbers and wall temperatures have been performed and the characteristics of TCI in pure air remain as those described in this paper. It is also shown that the nondimensional governing parameters 'interaction' Damköhler number and relative heat release provide a good metric for estimating the influence of TCI on the turbulence flow fields.

The insignificant influence of TCI on the turbulent flow dynamics for hypersonic boundary layers is different from what have been found for many combustion flows, as described in Section I. Possible reasons for the difference is that for combustions flows reaction intermediates like 'radicals' generally play an important role for the propagation of the overall reaction scheme, and a subtle change in the concentration of such radicals by turbulent fluctuations might substantially change the overall reaction rate and corresponding heat release rate. While for the air reaction mechanism used in the current analysis, this is not the case. In addition, air reactions happen at significantly higher temperatures ($T > 2500$K) than those for typical combustion applications. As a result, higher sensible enthalpy is necessary to intialize the air reactions, and the relative importance of chemical heat release due to TCI diminishes because of the higher flow enthalpy.

In addition, we present a PDF-TS approach to estimate the intensity of turbulence-chemistry interaction. This approach combines an assumed PDF with a temperature fluctuation scaling, named as PDF-TS. The assumed PDF is chosen to be either Gaussian or Beta, and the temperature fluctuation scaling is derived based on well-established boundary-layer relations. For RANS calculations with TCI neglected, PDF-TS provides a sanity check on whether TCI is negligible. It can also be used to identify regions where TCI could be potentially important, thus providing guidance on whether or not to undertake further efforts to model TCI under selected flow conditions.

IX. Acknowledgment

This work is sponsored by NASA under Cooperative Agreement NNX08AD04A under Dr. Peter Gnoffo, who the authors acknowledge for insightful discussions and the selection and assessment of flow conditions for the present studies.

References

[1]Libby, P. and Williams, F., "Turbulent Reacting Flows," *Academic Press, New York*, 1994.

[2]Gaffney, R., White, J., Girimaji, S., and Drummond, J., "Modeling temperature and species fluctuations in turbulent reacting flow," *Computing Systems in Engineering*, Vol. 5, No. 2, 1994, pp. 117–133.

[3]Delarue, B. and Pope, S., "Calculations of subsonic and supersonic turbulent reacting mixing layers using probability density function methods," *Physics of Fluids*, Vol. 10, No. 2, 1998, pp. 487–498.

[4]Hsu, A., Tsai, Y.-L., and Raju, M., "Probability density function approach for compressible turbulent reacting flows," *AIAA Journal*, Vol. 32, No. 7, 1994, pp. 1407–1415.

[5]Calhoon, W. and Kenzakowski, D., "Assessment of turbulence-chemistry interactions in missile exhaust plume signature," *Journal of Spacecraft*, Vol. 40, No. 5, 2003, pp. 694–695.

[6]Baurle, R. and Girimaji, S., "Assumed PDF turbulence-chemistry closure with temperature-composition correlations," *Combustion and Flames*, Vol. 134, 2003, pp. 131–148.

[7]Gerlinger, P., Noll, B., and Aigner, M., "Assumed PDF modeling and PDF structure investigation using finite-rate chemistry," *Progress in computational fluid dynamics*, Vol. 5, 2005, pp. 334–344.

[8]Guarini, S. E., Moser, R. D., Shariff, K., and Wray, A., "Direct numerical simulation of a supersonic turbulent boundary layer at Mach 2.5," *J. Fluid Mech.*, Vol. 414, 2000, pp. 1–33.

[9]Pirozzoli, S., Grasso, F., and Gatski, T. B., "Direct numerical simulation and analysis of a spatially evolving supersonic turbulent boundary layer at M = 2.25," *Physics of Fluids*, Vol. 16, No. 3, 2004, pp. 530–545.

[10]Maeder, T., Adams, N. A., and Kleiser, L., "Direct simulation of turbulent supersonic boundary layers by an extended temporal approach," *Journal of Fluid Mechanics*, Vol. 429, 2001, pp. 187–216.

[11]Duan, L., Beekman, I., and Martín, M. P., "Direct numerical simulation of hypersonic turbulent boundary layers. Part 2: Effect of temperature," *Journal of Fluid Mechanics*, Vol. 655, 2010, pp. 419–445.

[12]Duan, L., Beekman, I., and Martín, M. P., "Direct numerical simulation of hypersonic turbulent boundary layers. Part 3: Effect of Mach number," *Journal of Fluid Mechanics*, Vol. 672, 2011, pp. 245–267.

[13]Dong, M. and Zhou, H., "The improvement of turbulence modeling for the aerothermal computation of hypersonic turbulent boundary layers," *Science China*, Vol. 53, No. 2, 2010, pp. 369–379.

[14]Martin, M. and Candler, G., "Temperature Fluctuation Scaling in Reacting Turbulent Boundary Layers," *AIAA Paper No.01-2717*, 2001.

[15]Martin, M., "Exploratory Studies of Turbulence/Chemistry Interaction in Hypersonic Flows," *AIAA Paper No. 03-4055*, 2003.

[16]Duan, L. and Martin, M., "Effect of finite-rate chemistry reactions on turbulence in hypersonic turbulent boundary layers," *AIAA paper, No. 2009-588*, 2009.

[17]Duan, L. and Martin, M., "Effect of turbulence fluctuations on surface heating rate in hypersonic turbulent boundary layers," *AIAA paper, No. 2009-4040*, 2009.

[18]Wright, M., "DPLR CFD code," *NASA Ames Research Center, Moffett Field CA*.

[19]Duan, L. and Martin, M., "An effective procedure for testing the validity of DNS of wall-bounded turbulence including finite-rate reactions," *AIAA Journal*, Vol. 47, No. 1, 2009, pp. 244–251.

[20]Gordon, S. and McBride, B., "Computer Program for Calculation of Complex Chemical Equilibrium Compositions and Applications," *NASA Reference Publication 1311*, 1994.

[21]Gupta, R., Yos, J., Thompson, R., and Lee, K., "A Review of Reaction Rates and Thermodynamic and Transport Properties for 11-Species Air Model for Chemical and Thermal Non-equilibrium Calculations to 30000K," *NASA RP-1232*, 1990.

[22]Yos, J., "Transport properties of nitrogen, hydrogen, oxygen, and air to 30,000 K," *Avco. Corp. TR AD-TM-63-7*, 1963.

[23]Martin, M. and Candler, G., "A Parallel Implicit Method for the Direct Numerical Simulation of Compressible Flows," *Journal of Computational Physics*, Vol. 215, No. 1, 2006, pp. 153–171.

[24]Taylor, E., Wu, M., and Martin, M., "Optimization of Nonlinear Error Sources for Weighted Non-Oscillatory Methods in Direct Numerical Simulations of Compressible Turbulence," *Journal of Computational Physics*, Vol. 223, 2006, pp. 384–397.

[25]Williamson, J., "Low-storage Runge-Kutta Schemes," *Journal of Computational Physics*, Vol. 35(1), 1980, pp. 48–56.

[26]Martin, M., "DNS of Hypersonic Turbulent Boundary Layers. Part I: Initialization and Comparison with Experiments," *Journal of Fluid Mechanics*, Vol. 570, 2007, pp. 347–364.

[27]Park, C., "Non-equilibrium Hypersonic Aerodynamics," *Wiley*, 1990.

[28]Martin, M. and Candler, G., "Effect of Chemical Reactions on Decaying Isotropic Turbulence," *Physics of Fluids*, Vol. 10, No. 7, 1998, pp. 1715–1724.

[29]Martin, M. and Candler, G., "Subgrid-scale model for the temperature fluctuations in reacting hypersonic turbulent flows," *Physics of Fluids*, Vol. 11, No. 9, 1999, pp. 2765–2771.

[30]Baurle, R., "Modeling of high speed reacting flows: established practices and future challenges," *AIAA Paper No.2004-0267*, 2000.

[31]S.H.Frankel, J.P.Drummond, and H.A.Hassan, "A hybrid Reynolds averaged/PDF closure model for supersonic turbulent combustion," *AIAA Paper No. 1990-1573*, 1990.

[32]R.L.Gaffney, J.A.White, S.S.Girimaji, and J.P.Drummond, "Modeling turbulent/chemistry interactions using assumed PDF Methods," *AIAA Paper No. 1992-3638*, 1992.

[33]Huang, P. G., Coleman, G. N., and Bradshaw, P., "Compressible turbulent channel flows: DNS results and modelling," *Journal of Fluid Mechanics*, Vol. 305, 1995, pp. 185–218.

[34]Duan, L. and Martín, M., "Direct numerical simulation of hypersonic turbulent boundary layers. Part 4: Effects of high enthalpy," *accepted for publication by Journal of Fluid Mechanics*, 2011.

[35]Gaviglio, J., "Reynolds analogies and experimental study of heat transfer in the supersonic boundary layer," *International Journal of Heat and Mass Transfer*, Vol. 30, No. 5, 1987, pp. 911–926.

[36]Wilcox, D. C., *Turbulence Modeling for CFD*, DCW Industries, Inc., La Canada, CA, 3rd ed., 2006.

[37]Baurle, R., *Modeling of turbulent reacting flows with probability density function for scramjet applications*, Ph.D. thesis, North Carolina State University, Raleigh, NC, 1995.

[38]Bray, K. and Moss, J., "A unified statistical model of premixed turbulent flames," *Acta Astronaut*, Vol. 4, 1977, pp. 291–319.

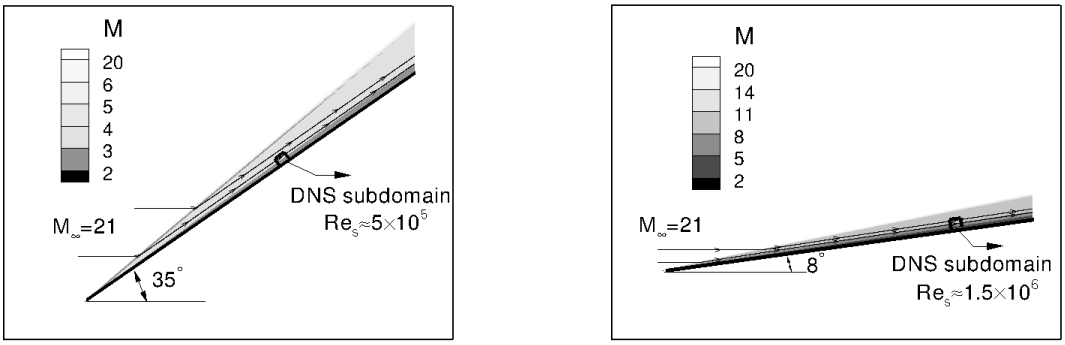

Figure 1. DNS subdomain from RANS solution for the study of turbulence-chemistry interaction. The Reynolds number $Re_s = \frac{\rho_\infty u_\infty s}{\mu_\infty}$ with s the distance between the leading edge of the lifting body to the location of the DNS subdomain.

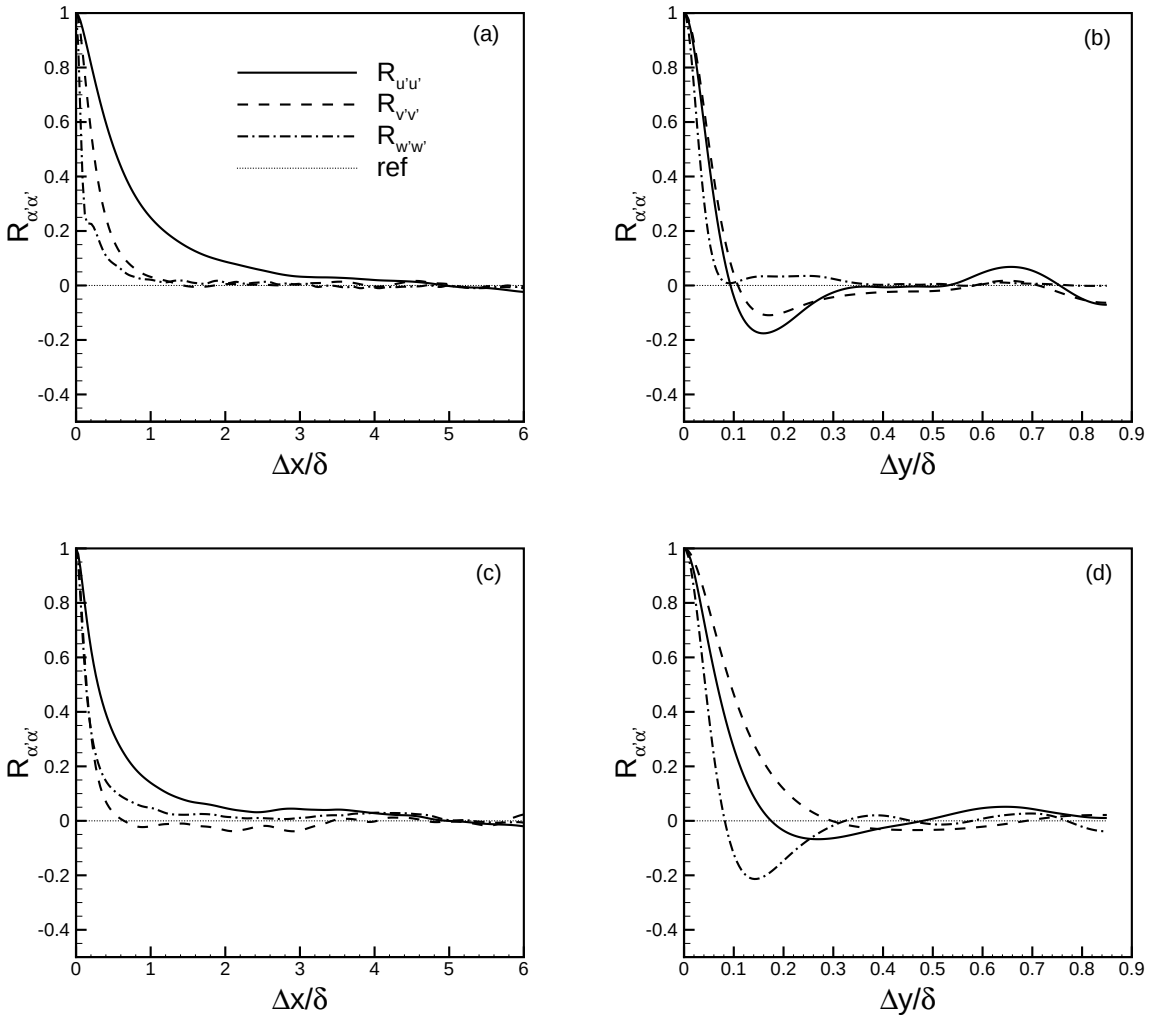

Figure 2. Two-point correlations $R_{\alpha'\alpha'}$ for streamwise, spanwise and wall-normal velocity components for Wedge35supercata. Plotted versus (*a*) $\Delta x/\delta$ at $z^+ = 15$, (*b*) $\Delta y/\delta$ at $z^+ = 15$; (*c*) $\Delta x/\delta$ at $z/\delta = 0.1$; (*d*) $\Delta y/\delta$ at $z/\delta = 0.1$.

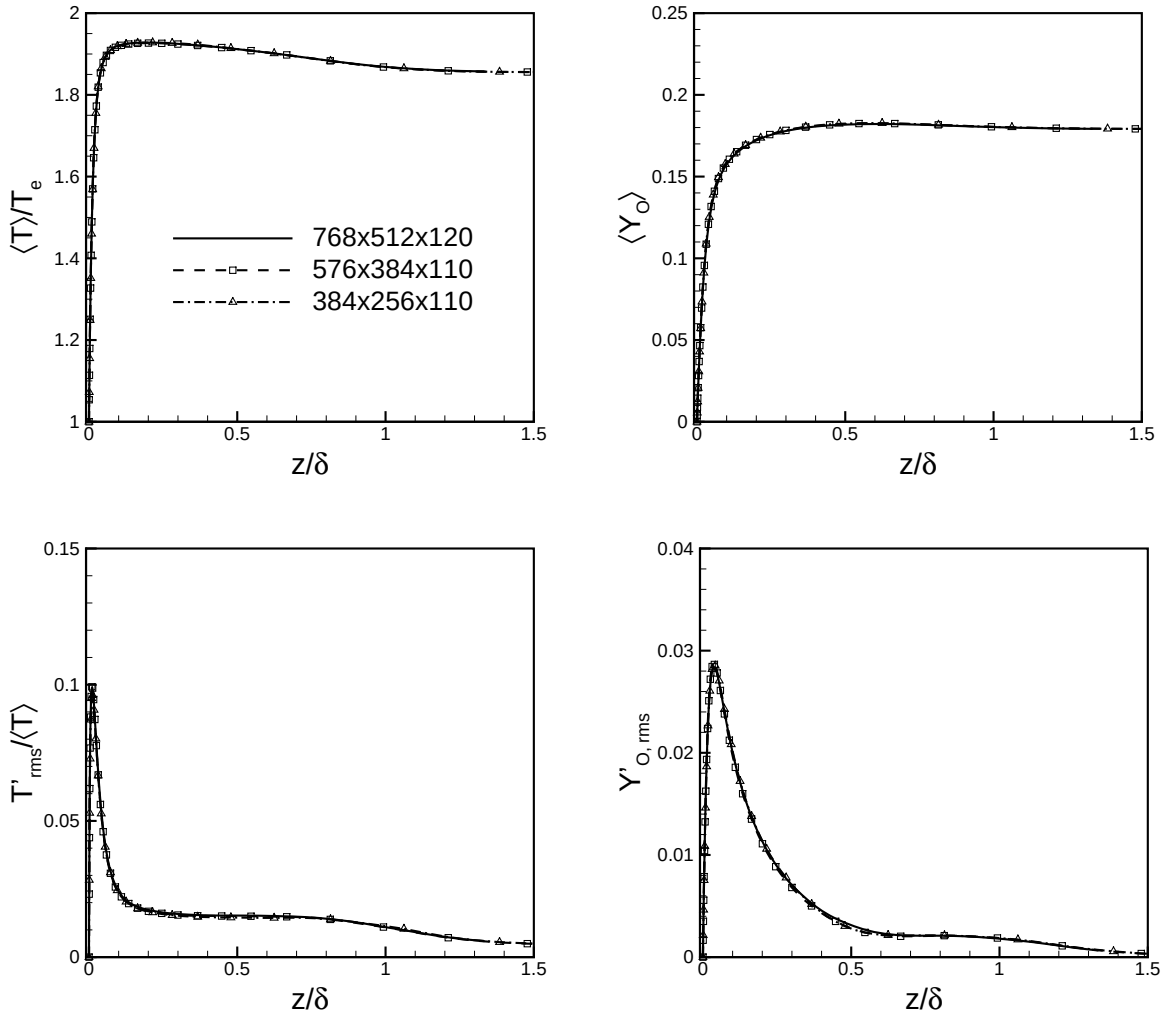

Figure 3. Convergence study for Wedge35supercata varying grid size, $N_x \times N_y \times N_z$.

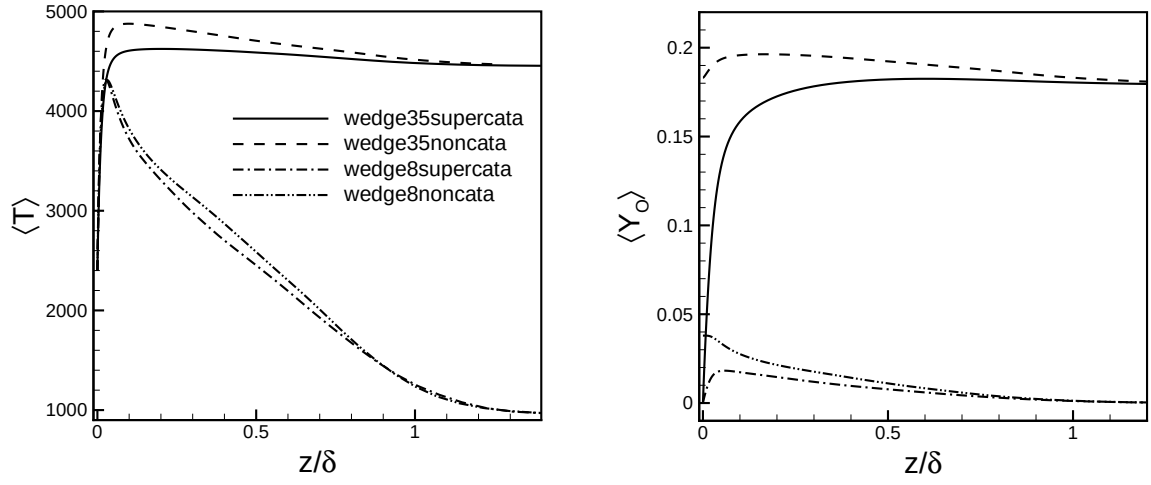

Figure 4. Mean profiles for temperature and atomic oxygen mass fraction for various cases.

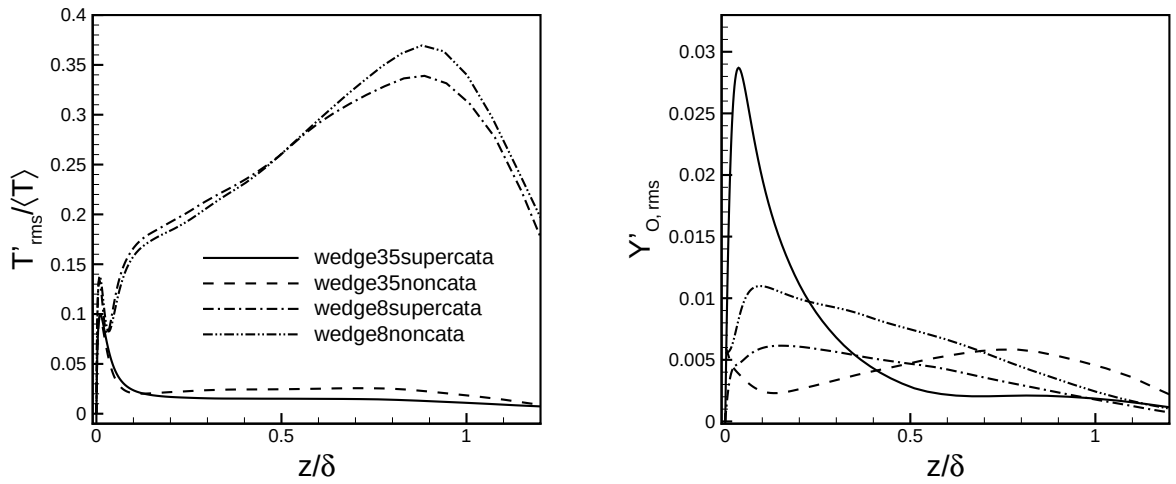

Figure 5. RMS of fluctuations in temperature and atomic oxygen mass fraction for various cases.

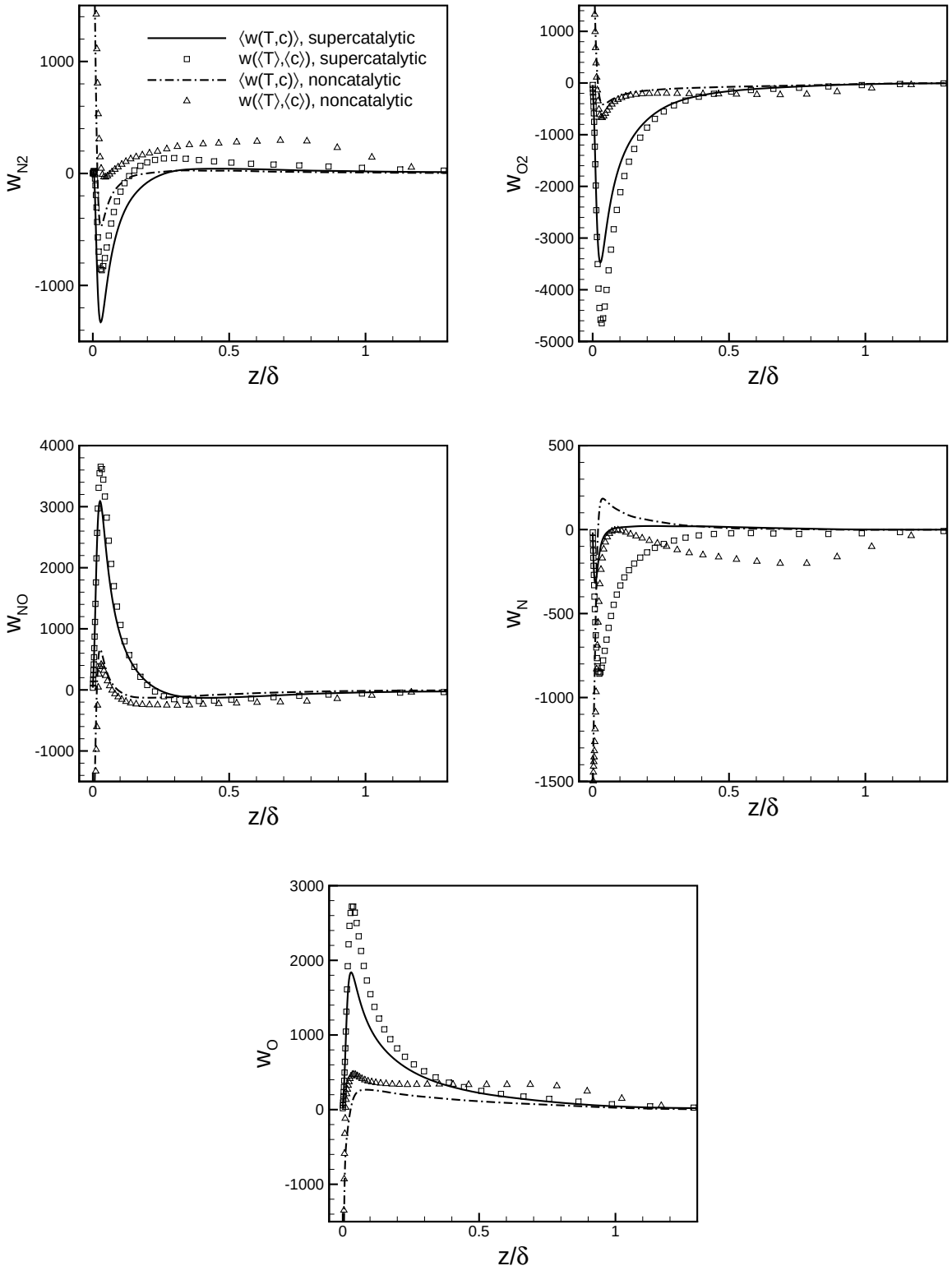

Figure 6. 'Turbulent' and 'laminar' chemical production rates of various species for Wedge35.

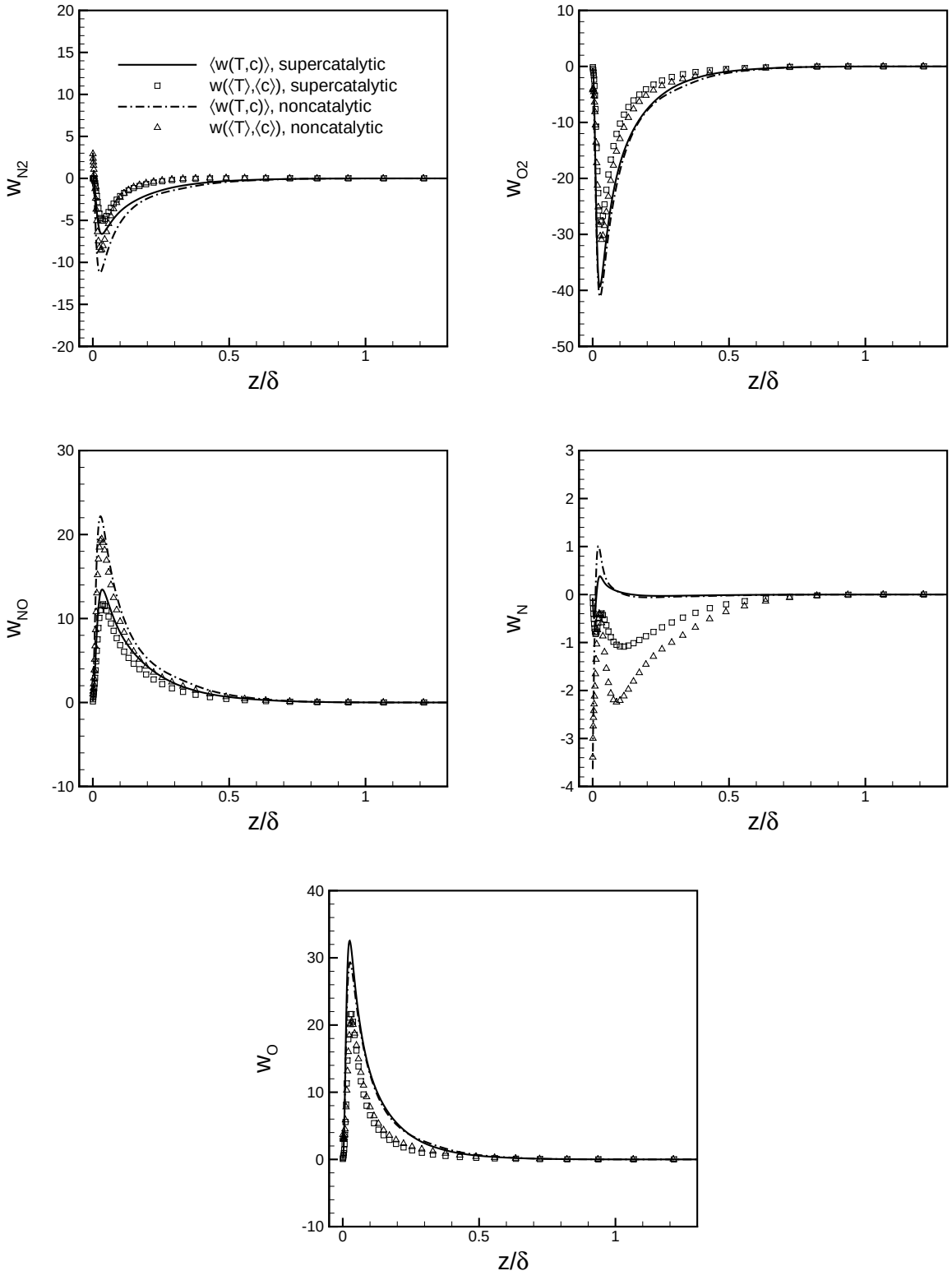

Figure 7. 'Turbulent' and 'laminar' chemical production rates of various species for Wedge8.

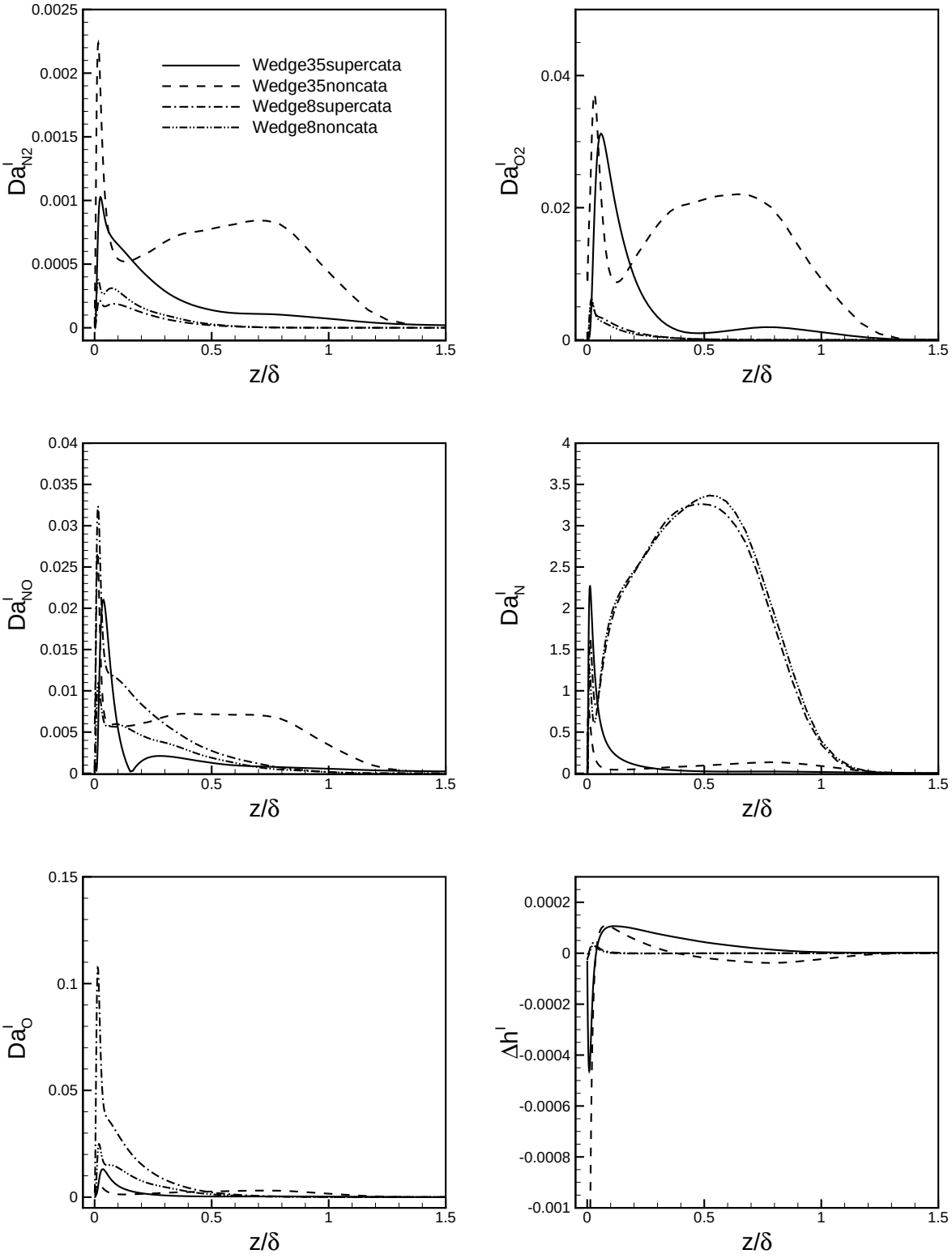

Figure 8. Da_s^I **and** $\overline{\Delta h^I}$ **across the boundary layer.**

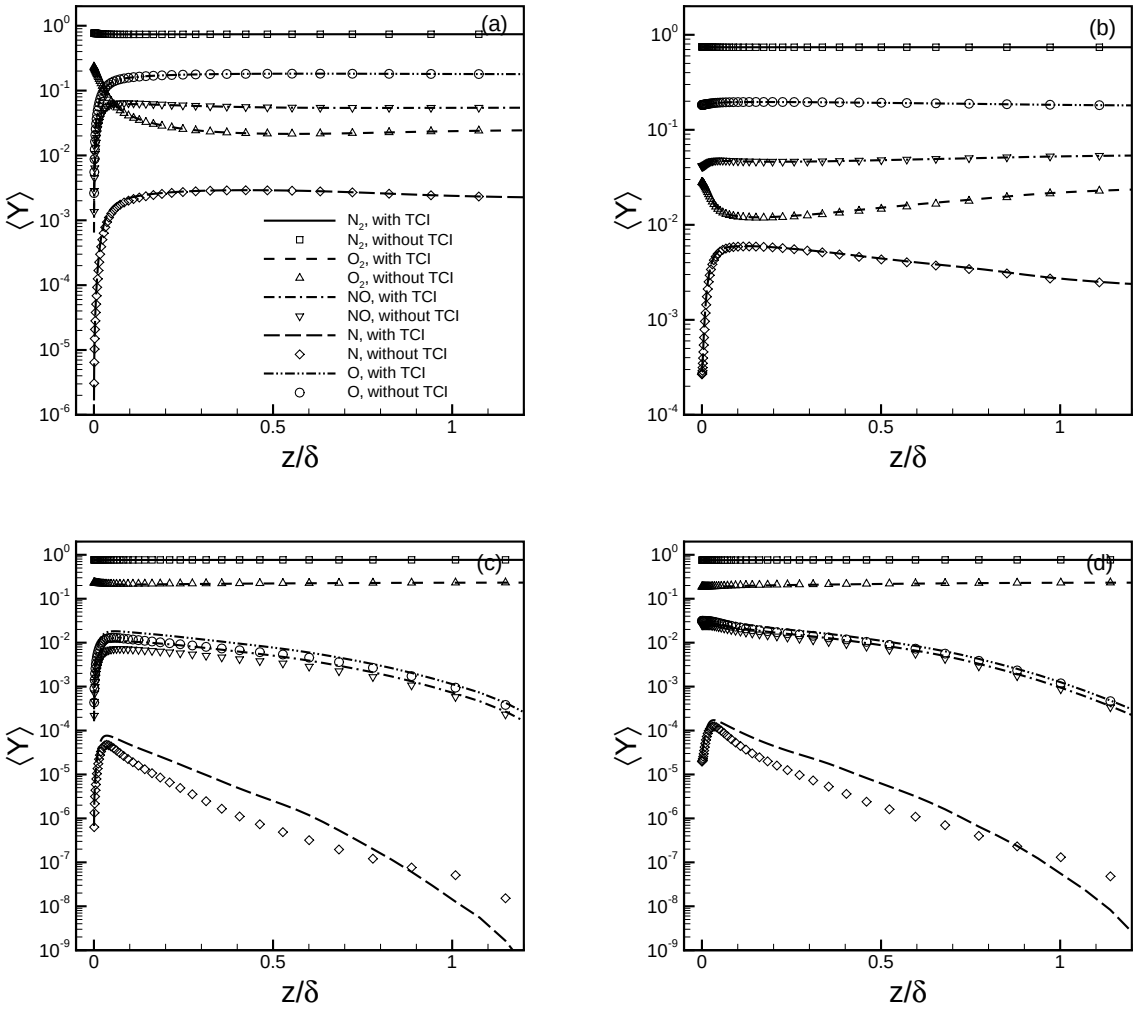

Figure 9. Mean species mass fraction for various cases with and without TCI. (a) Wedge35supercata, (b) Wedge35noncata, (c) Wedge8supercata, (d) Wedge8noncata.

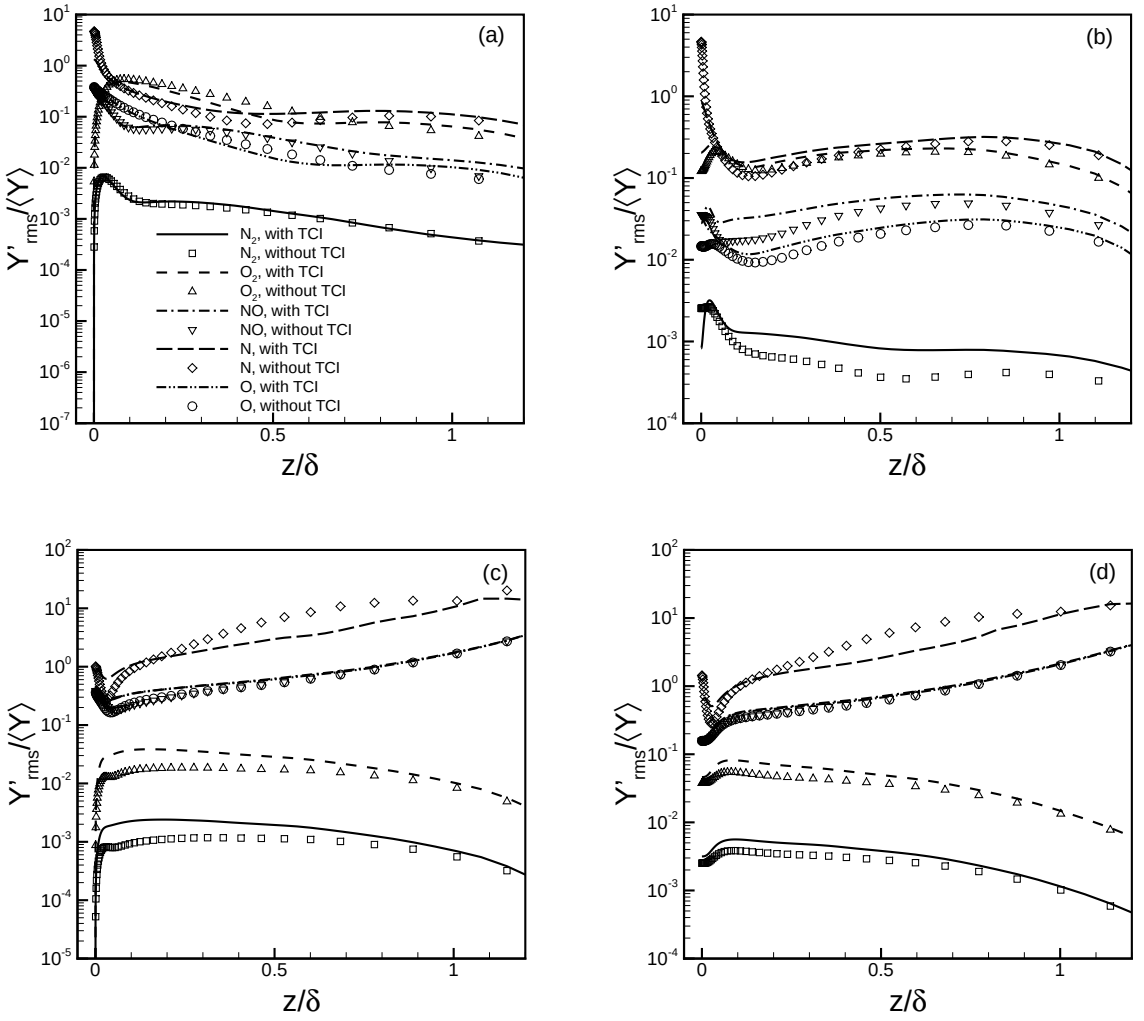

Figure 10. RMS of species mass fraction for various cases with and without TCI. (a) Wedge35supercata, (b) Wedge35noncata, (c) Wedge8supercata, (d) Wedge8noncata.

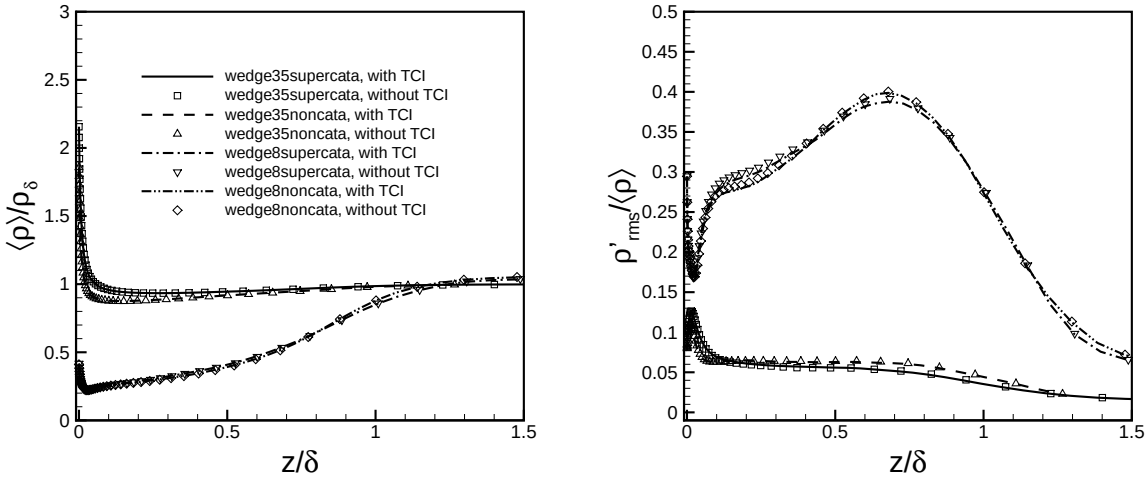

Figure 11. Mean and RMS of total density across the boundary layer with and without TCI.

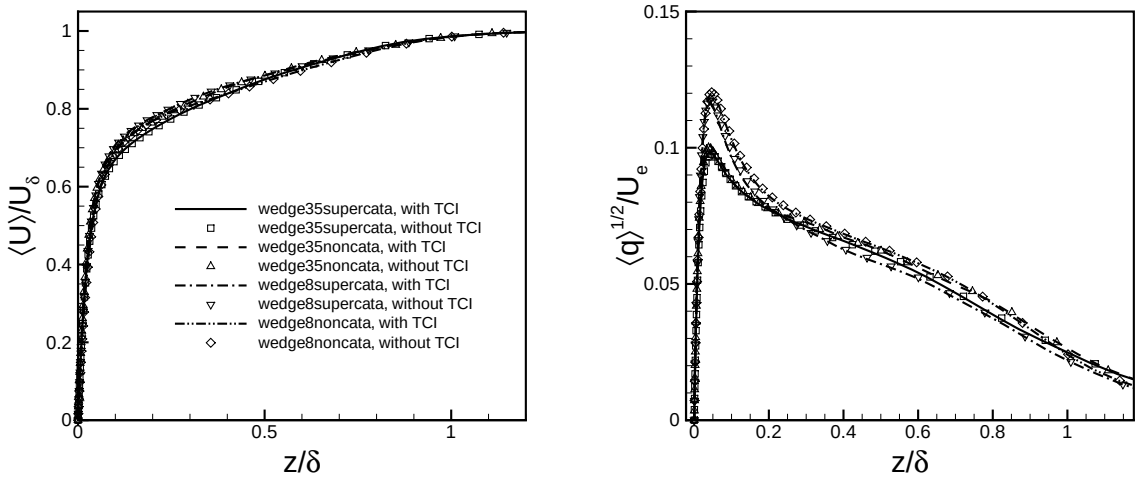

Figure 12. Mean streamwise velocity and turbulent kinetic energy across the boundary layer with and without TCI.

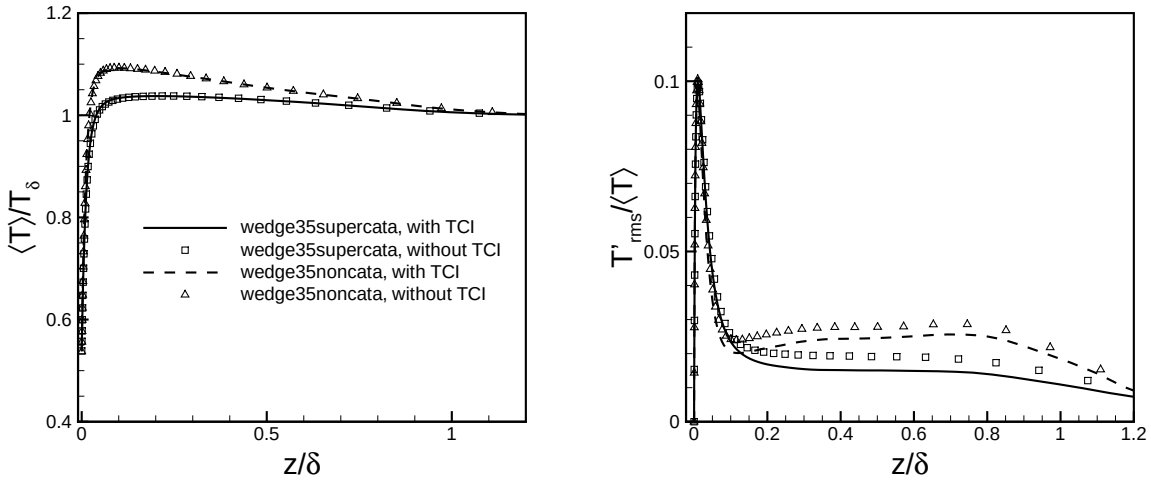

Figure 13. Mean and RMS of temperature across the boundary layer with and without TCI for Wedge35.

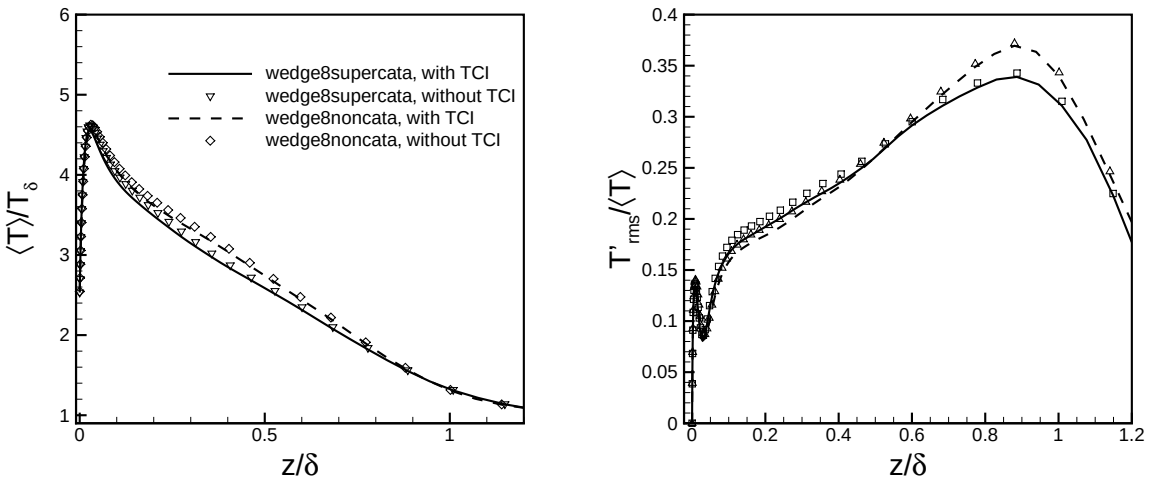

Figure 14. Mean and RMS of temperature across the boundary layer with and without TCI for Wedge8.

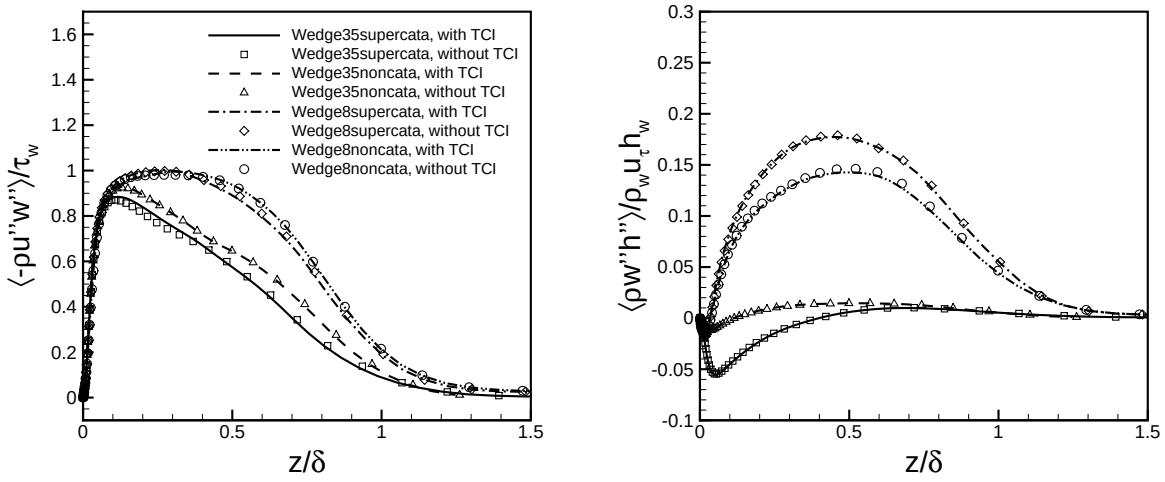

Figure 15. Reynolds shear stress $\overline{\rho u'' w''}/\tau_w$ and turbulent heat flux $\overline{\rho w'' h''}/\overline{\rho}_w u_\tau \overline{h}_w$ across the boundary layer with and without TCI.

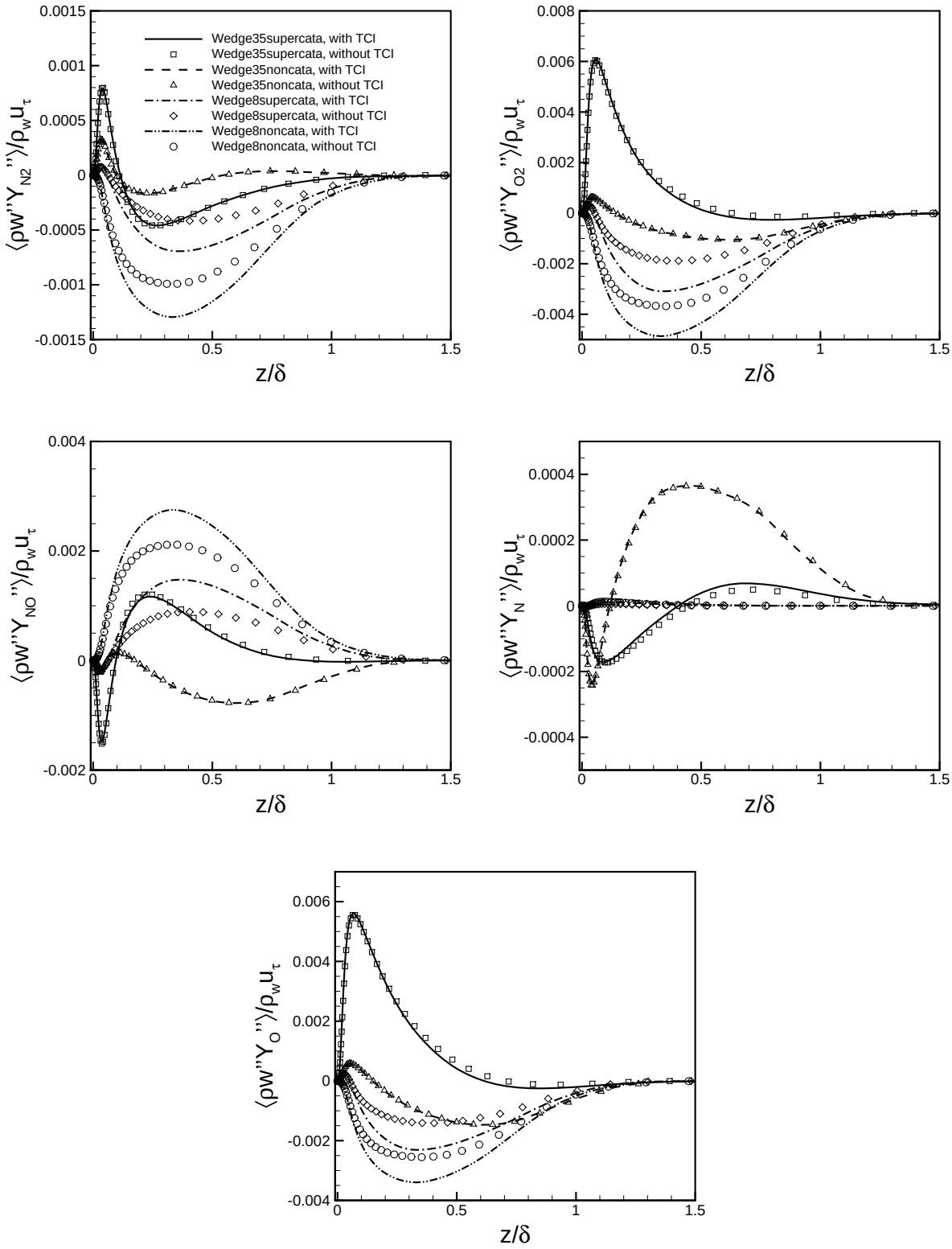

Figure 16. Turbulent mass flux $\overline{\overline{\rho} w'' Y''} / \overline{\rho}_w u_\tau$ for various species with and without TCI.

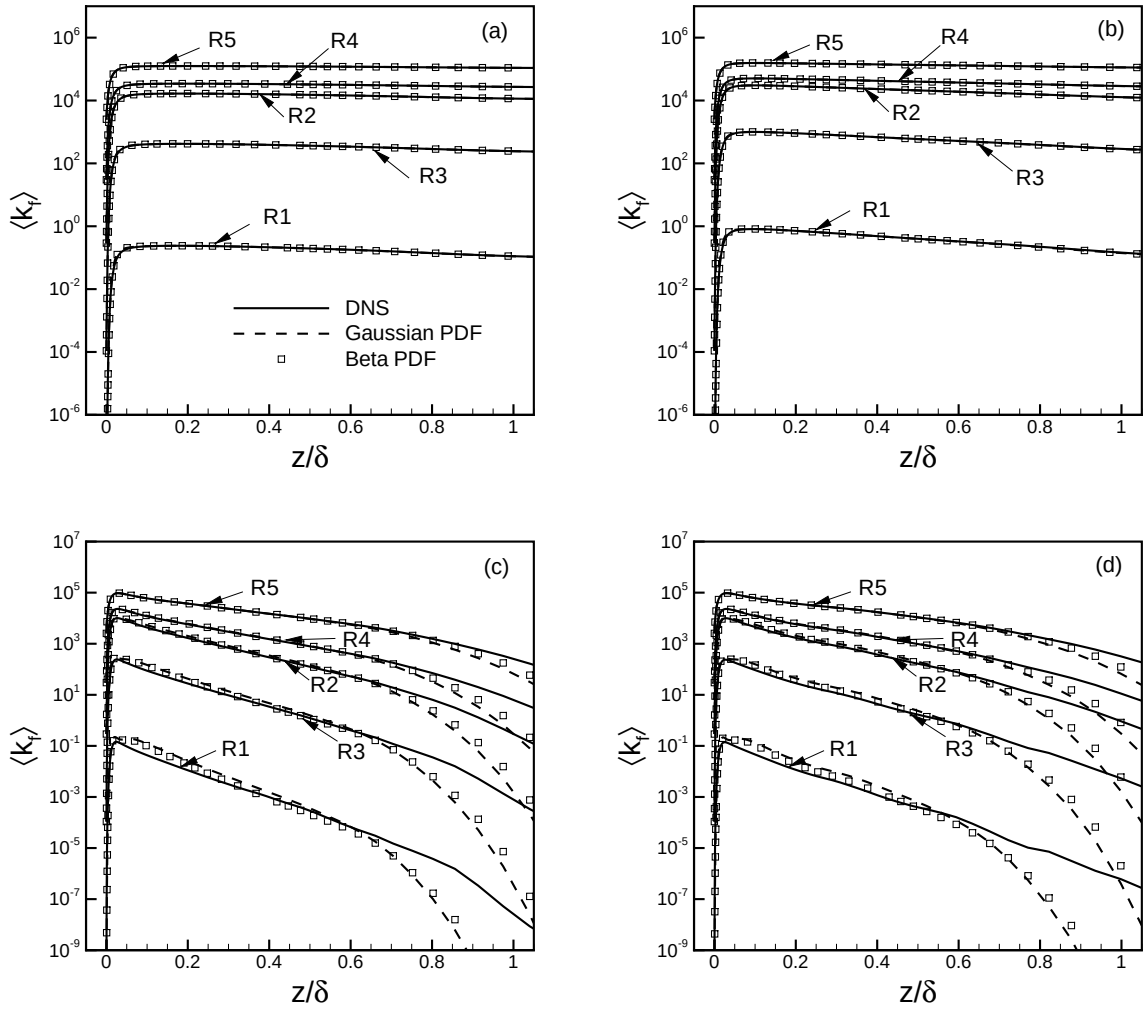

Figure 17. Mean forward reaction rate constants computed by averaging DNS flow fields and assumed PDF methods. (*a*) Wedge35supercata; (*b*) Wedge35noncata; (*c*) Wedge8supercata; (*d*) Wedge8noncata.

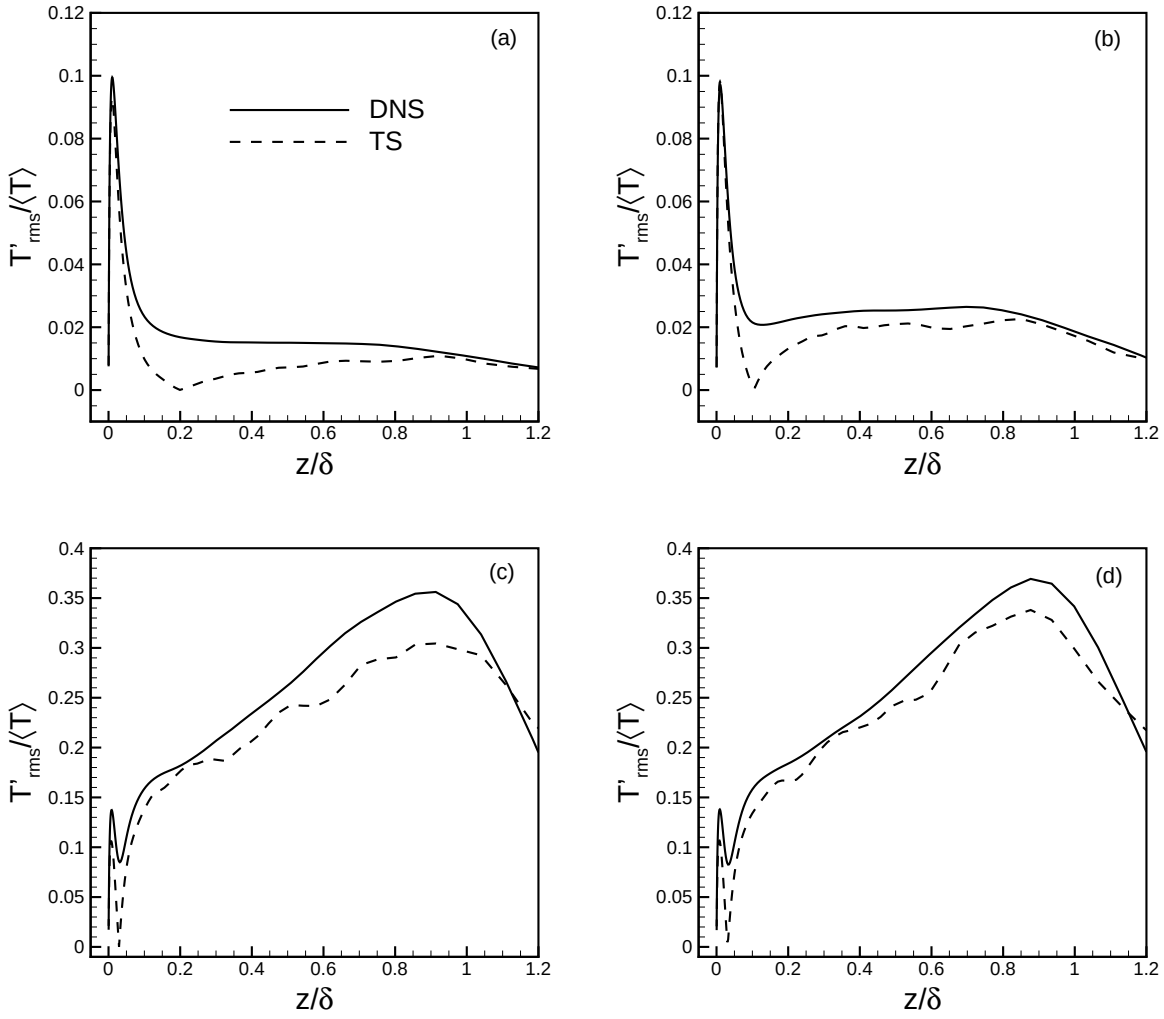

Figure 18. Temperature fluctuation intensity computed using DNS flow fields or the temperature fluctuation scaling given by Equation 20. Constant Pr_t is assumed with value 1.0 in the temperature fluctuation scaling. (a) Wedge35supercata; (b) Wedge35noncata; (c) Wedge8supercata; (d) Wedge8noncata.

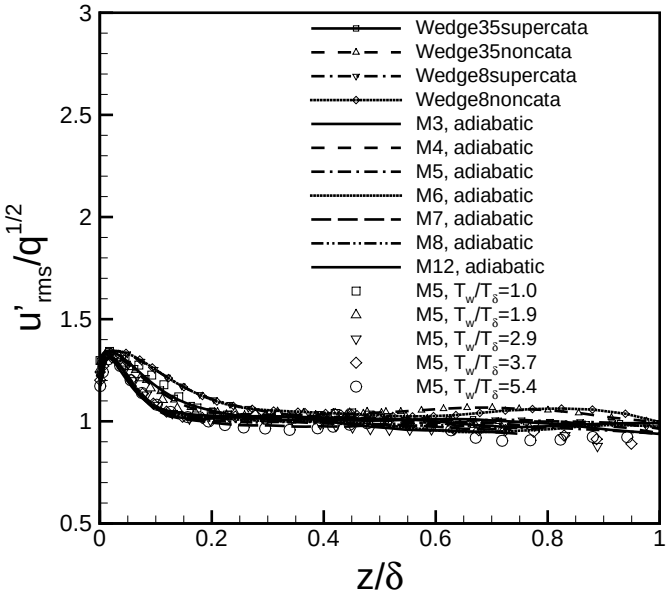

Figure 19. $u'_{rms}/q^{1/2}$ **computed using DNS flow fields with varying freestream Mach number, wall temperature and enthalpy conditions.**[11,12]

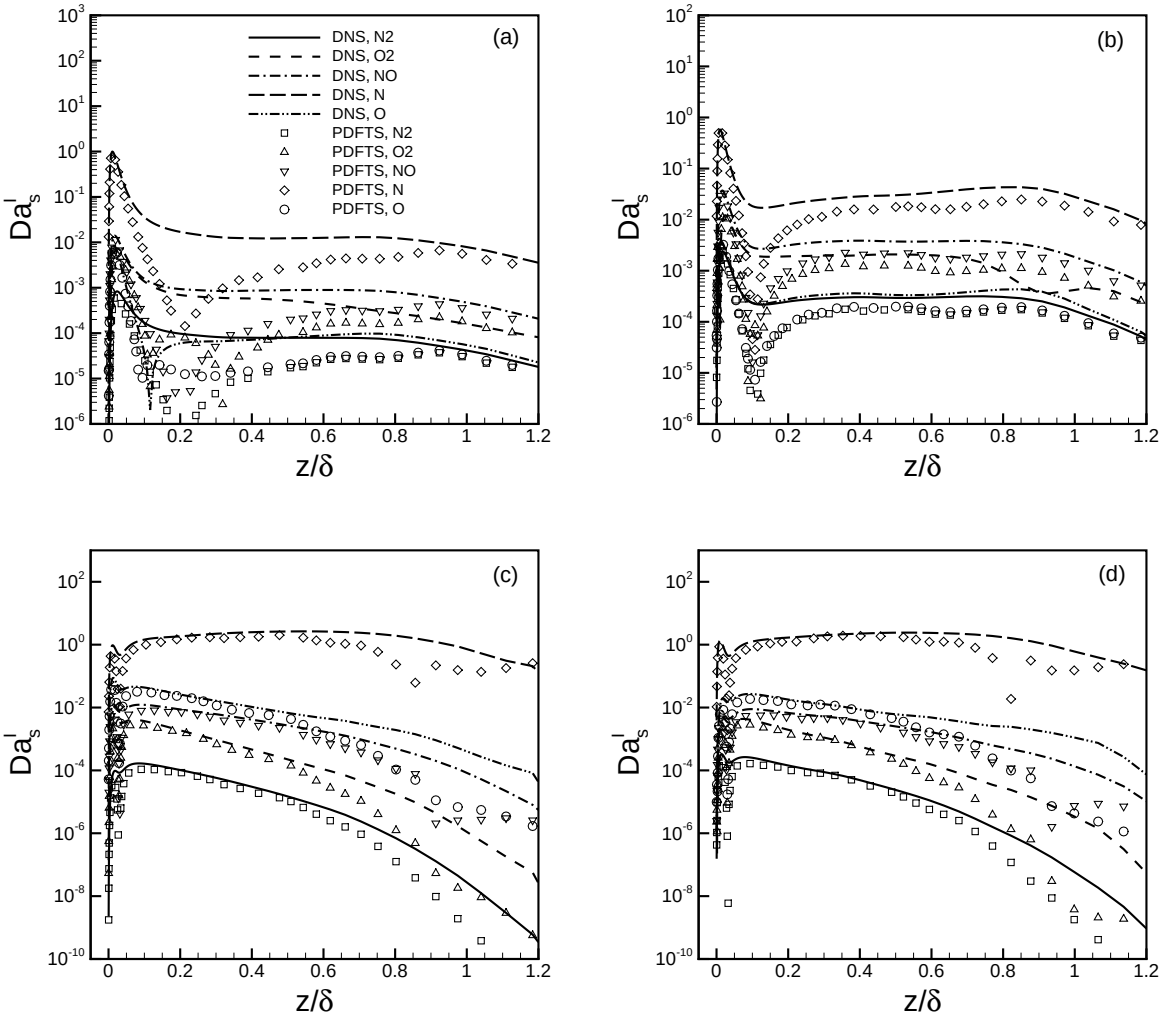

Figure 20. 'Interaction' Damköhler number Da_s^I ((Equation 11) computed by averaging DNS flow fields and PDF-TS method. The PDF-TS method combines the Gaussian PDF given by Equation 14 and the temperature scaling given by Equation 22 with $Pr_t = 1.0$ and the value C_M given by Equation 24. (a) Wedge35supercata; (b) Wedge35noncata; (c) Wedge8supercata; (d) Wedge8noncata.

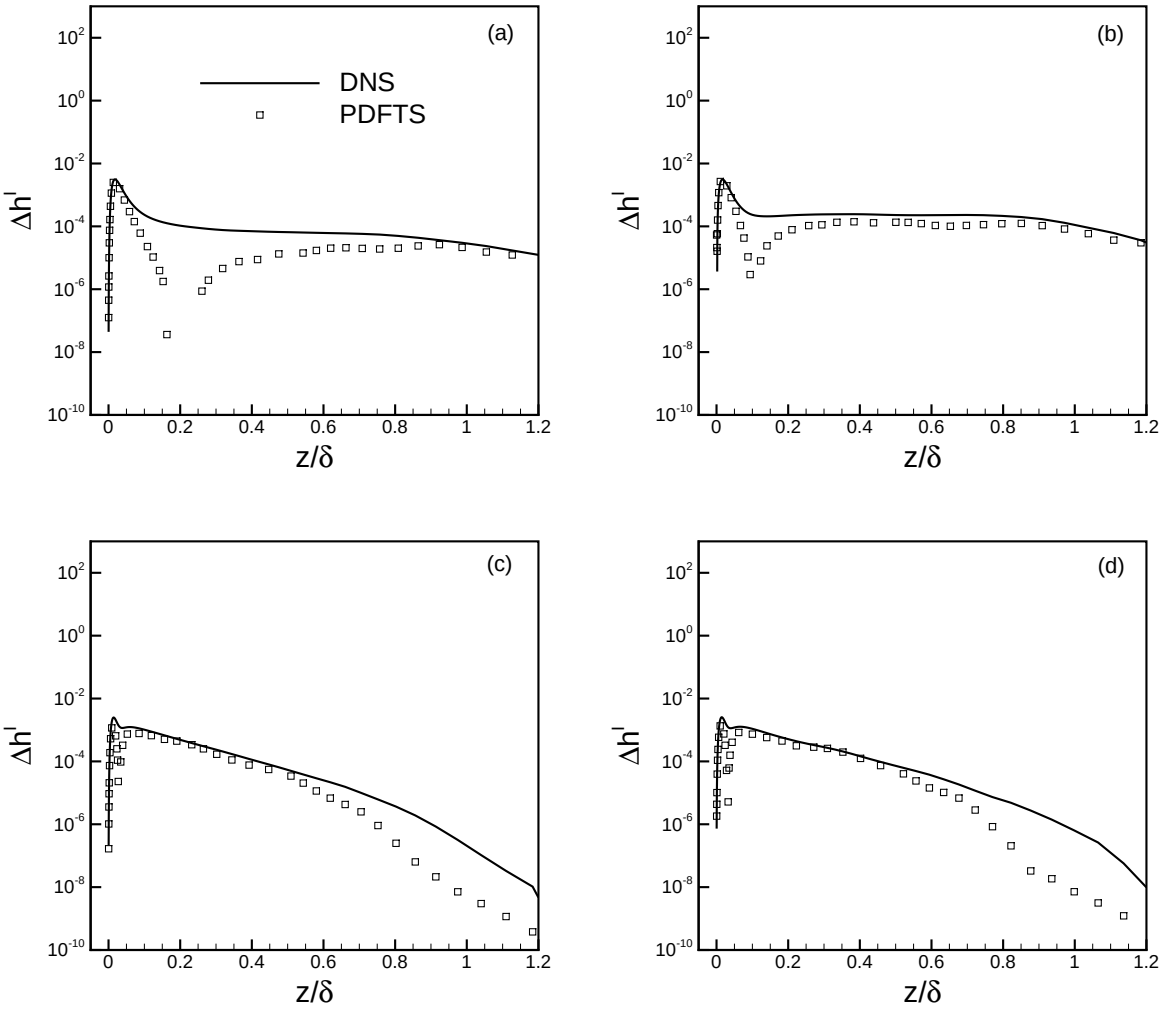

Figure 21. 'Interaction' relative heat release $\overline{\Delta h}^I$ (Equation 11) computed by averaging DNS flow fields and PDF-TS method. The PDF-TS method combines the Gaussian PDF given by Equation 14 and the temperature scaling given by Equation 22 with $Pr_t = 1.0$ and the value C_M given by Equation 24. (*a*) Wedge35supercata; (*b*) Wedge35noncata; (*c*) Wedge8supercata; (*d*) Wedge8noncata.